Heliyon 10 (2024) e34756

Contents lists available at ScienceDirect

Heliyon

journal homepage: www.cell.com/heliyon

Research article

The genomic mosaic of mitochondrial dysfunction: Decoding nuclear and mitochondrial epigenetic contributions to maternally inherited diabetes and deafness pathogenesis

Luigi Donato [a,b], Concetta Scimone [a,b], Simona Alibrandi [a,b,*], Maria Vadalà [b,c], Massimo Castellucci [c], Vincenza Maria Elena Bonfiglio [c], Sergio Zaccaria Scalinci [d], Giorgia Abate [a], Rosalia D'Angelo [a], Antonina Sidoti [a]

[a] Department of Biomedical and Dental Sciences and Morphofunctional Imaging, Division of Medical Biotechnologies and Preventive Medicine, University of Messina, Messina, 98125, Italy
[b] Department of Biomolecular Strategies, Genetics and Cutting-edge Therapies, I.E.ME.S.T., Palermo, 90139, Italy
[c] Department of Biomedicine, Neuroscience and Advanced Diagnostic (BIND), Ophthalmology Institute, University of Palermo, 90143, Palermo, Italy
[d] Department of Medical and Surgical Sciences, University of Bologna, Bologna, 40121, Italy

ARTICLE INFO

Keywords:
mtDNA
WGS
WES
Epigenetics
MIDD

ABSTRACT

Aims: Maternally inherited diabetes and deafness (MIDD) is a complex disorder characterized by multiorgan clinical manifestations, including diabetes, hearing loss, and ophthalmic complications. This pilot study aimed to elucidate the intricate interplay between nuclear and mitochondrial genetics, epigenetic modifications, and their potential implications in the pathogenesis of MIDD.

Main methods: A comprehensive genomic approach was employed to analyze a Sicilian family affected by clinically characterized MIDD, negative to the only known causative m.3243 A > G variant, integrating whole-exome sequencing and whole-genome bisulfite sequencing of both nuclear and mitochondrial analyses.

Key findings: Rare and deleterious variants were identified across multiple nuclear genes involved in retinal homeostasis, mitochondrial function, and epigenetic regulation, while complementary mitochondrial DNA analysis revealed a rich tapestry of genetic diversity across genes encoding components of the electron transport chain and ATP synthesis machinery. Epigenetic analyses uncovered significant differentially methylated regions across the genome and within the mitochondrial genome, suggesting a nuanced landscape of epigenetic modulation.

Significance: The integration of genetic and epigenetic data highlighted the potential crosstalk between nuclear and mitochondrial regulation, with specific mtDNA variants influencing methylation patterns and potentially impacting the expression and regulation of mitochondrial genes. This pilot study provides valuable insights into the complex molecular mechanisms underlying MIDD, emphasizing the interplay between nucleus and mitochondrion, tracing the way for future research into targeted therapeutic interventions and personalized approaches for disease management.

* Corresponding author. Department of Biomedical and Dental Sciences and Morphofunctional Imaging, Division of Medical Biotechnologies and Preventive Medicine, University of Messina, Messina, 98125, Italy.
E-mail address: salibrandi@unime.it (S. Alibrandi).

https://doi.org/10.1016/j.heliyon.2024.e34756
Received 29 June 2024; Received in revised form 16 July 2024; Accepted 16 July 2024
Available online 17 July 2024

Abbreviations

MIDD	Maternally Inherited Diabetes and Deafness
WES	Whole-Exome Sequencing
WGBS	Whole-Genome Bisulfite Sequencing
mtDNA	Mitochondrial DNA
DM	Diabetes Mellitus
BMI	Body Mass Index
RPE	Retinal Pigment Epithelium
CC	Choriocapillaris
ERG	Electroretinography
ATP	Adenosine Triphosphate
tRNAs	Transfer RNAs
rRNAs	Ribosomal RNAs
WGS	Whole Genome Sequencing
FA	Fluorescein Angiography
FAF	Fundus Autofluorescence
OCT	Optical Coherence Tomography
SS-OCT	Swept Source Optical Coherence Tomography
PCR	Polymerase Chain Reaction
gDNA	Genomic DNA
GATK	Genome Analysis Toolkit
ANNOVAR	Annotate Variation
HGMD	Human Gene Mutation Database
LOVD	Leiden Open Variation Database
RetNet	Retinal Network
UTRs	Untranslated Regions
MSeqDR	Mitochondrial Disease Sequence Data Resource
SIFT	Sorting Intolerant From Tolerant
PhyloP	Phylogenetic P-values
PhastCons	Phylogenetic Analysis with Space/Time Conservation
BWA	Burrows-Wheeler Aligner
GO	Gene Ontology
KEGG	Kyoto Encyclopedia of Genes and Genomes
FDR	False Discovery Rate
ROC	Receiver Operating Characteristic
MALDI-TOF	Matrix-Assisted Laser Desorption/Ionization Time of Flight
DSB	Double-Strand Break
NGS	Next-Generation Sequencing
SSCP	Single-Strand Conformation Polymorphism
DMR	Differentially Methylated Region
SAGE	Serial Analysis of Gene Expression
CpG	Cytosine-phosphate-Guanine
HPLC	High-Performance Liquid Chromatography
RT-qPCR	Real-Time Quantitative PCR
TFIIH	Transcription Factor II Human
ROS	Reactive Oxygen Species
MMXD	MMS19-MIP18-XPD
mTORC	Mechanistic Target of Rapamycin Complex
HmtVAR	Human Mitochondrial Variation
CPD	Compensated Pathogenic Deviations
MISTIC	Mutual Information Score
EV	Evolutionary Variation
TSS	Transcription Start Site
TIR	Transcription Initiation Region
CpGI	CpG Island

1. Introduction

Maternally inherited diabetes and deafness (MIDD) is a rare, multisystemic disorder [1], first described in 1992, and affecting up to 1 % of patients with diabetes [2]. Diabetes mellitus (DM), deafness, ophthalmic disease, myopathies, cardiac disease, gastrointestinal disease, renal disease, and short stature constitute its most represented clinical symptoms. MIDD patients typically have insulin-dependent diabetes with relatively low body mass index (BMI), with diabetes onset occurring during the third or fourth decade of life. Insulin-dependence is usually correlated with progressive neurosensory deafness [3]. Ophthalmologically, MIDD patients often present with circumferentially oriented but discontinuous patches of retinal pigment epithelium (RPE) and choriocapillaris (CC) atrophy around the macula, within the arcades [4]. Corneal endothelial polymegathism is also commonly observed, while vision is typically good (20/40 or better). Full-field electroretinography (ERG) generally does not show generalized retinal dysfunction, but pattern ERG or multifocal ERG may reveal abnormal retinal function [5].

This disorder is primarily caused by mutations in the mitochondrial DNA (mtDNA), leading to impaired mitochondrial function and cellular energy production [6].

Mitochondria are essential organelles responsible for energy production through oxidative phosphorylation, and they play a crucial role in various cellular processes, including calcium homeostasis, apoptosis, and redox signaling [7]. The mitochondrial genome encodes 13 essential proteins that are part of the electron transport chain and ATP synthase complex, as well as 22 transfer RNAs (tRNAs) and 2 ribosomal RNAs (rRNAs) required for mitochondrial protein synthesis [8]. Mutations in the mtDNA can disrupt these critical components, leading to impaired mitochondrial function and cellular energy deficits [9,10].

The most common associated variant in MIDD is the m.3243A > G mutation in the tRNALeu gene [11]. Classically, the maternal inheritance of MIDD is attributed to the absence or near-absence of mitochondria in the sperm cell, leading to the exclusive inheritance of mitochondria from the oocyte [12]. However, the concept of paternal mitochondrial inheritance is currently being debated, with some suggesting the presence of a protease system that destroys paternal mtDNA upon entry into the oocyte [13].

Heteroplasmy, the coexistence of different copies of mtDNA within a cell, is another crucial factor to consider in the context of mitochondrial inheritance and disease manifestation [14]. Where mutated mtDNA copies predominate in specific body districts, the resulting phenotype is more likely to be symptomatic, while a lower representation of mutated copies reduces the probability of illness [15].

While mtDNA mutations are considered the primary genetic cause of MIDD, recent studies have suggested that variants in nuclear genes can also contribute to the pathogenesis of this disorder [16]. Nuclear genes play essential roles in various cellular processes, including mitochondrial biogenesis, maintenance, and quality control [17]. Mutations in these nuclear genes can indirectly impact mitochondrial function, further exacerbating the cellular energy deficits and dysfunction observed in MIDD [18].

In addition to genetic factors, epigenetic modifications, such as DNA methylation, have been implicated in the regulation of gene expression and cellular processes [19]. Alterations in DNA methylation patterns can affect the expression of both nuclear and mitochondrial genes, potentially contributing to the complex phenotypic manifestations observed in MIDD [20,21].

This study aims to elucidate the intricate interplay between nuclear and mitochondrial genetics, epigenetic modifications, and their potential implications in the pathogenesis of MIDD. Such complex pattern is at the basis of many other multigenic and multifactorial diseases involving at different levels the retina and its microenvironment [22]. By employing a comprehensive genomic approach, including whole-exome sequencing (WES), whole-genome bisulfite sequencing (WGBS), and mitochondrial DNA analysis, this research investigates the hypothesis that mutations and methylation alterations in both mitochondrial and nuclear genes could impair related molecular mechanisms, ultimately leading to the MIDD phenotype observed in a Sicilian family.

This study provides valuable insights into the complex molecular mechanisms underlying MIDD, emphasizing the potential crosstalk between nuclear and mitochondrial regulation, and paving the way for future research into targeted therapeutic interventions and personalized approaches for disease management.

2. Materials and methods

2.1. Family clinical data

A Sicilian family from Palermo, composed by four members, was examined. The proband is a 62-year-old female, who was admitted at the Eye Clinic of the University of Palermo for vision trouble. The evaluation included her 64-year-old husband, identified as II4, and the two daughters, 29 and 27 years old respectively, identify as III1 and III2 in Fig. 1 (see Results section). The proband's medical history reported deafness and type II diabetes and her biochemical assays demonstrated suboptimal glycemic regulation, resulting in recurrent admissions for diabetic ketosis or ketoacidosis. Starting from her clinical evaluation, her husband and her two daughters were asked to be examined.

Each member of the family was evaluated with a comprehensive ophthalmological evaluation, including visual acuity examination with the Snellen chart, slight lamp examination and tonometry, color vision with HRR and Ishihara pseudochromatic tables. All of them underwent an array of multimodal retinal diagnostic exams as follow: color fundus photography, optical coherence tomography (OCT), fluorescein angiography (FA) and fundus autofluorescence (FAF) for imaging retinal structures. High resolution swept source optical coherence tomography (SS-OCT) imaging was conducted using the DRI Triton OCT (Topcon, Japan), FA and FAF were performed by Visucam 500 (Carl Zeiss Meditec AG, Germany). Additionally, a detailed clinical history of the subjects' family members was collected, emphasizing the subjective perception of vision loss, age at onset, progression, pharmacological treatment, and the presence

of specific inherited retinal dystrophy (IRD) manifestations, including night vision deficits, peripheral vision loss, and alterations in color vision. This study was approved by the Scientific Ethics Committee of the "Azienda Policlinico Universitario di Messina" (approval number: 23/17bis, prot. n. 0014661). All procedures involving human participants were performed in accordance with institutional and/or national research committee ethical standards and performed in accordance with the 1964 Declaration of Helsinki and its later amendments or comparable ethical standards. The participants gave written informed consent for the publication of any images, clinical data and other data included in the manuscript.

2.2. Genotyping the m.3243A > G in family mtDNA

Mitochondrial DNA was isolated from the whole blood of participants using Abcam Mitochondrial DNA Isolation Kit (ab65321). The fragment spanning the m.3243A > G mutation of all family members was PCR-amplified with HotStarTaq Plus DNA Polymerase (Qiagen), by using 20 ng genomic DNA and 0.3 μM of each light-strand and heavy-strand oligonucleotide primers (forward primer 5′-ATTGACCTGCCCGTGAAGA-3′ and reverse primer 5′-GCAGGAGTAATCAGAGGTG-3′, annealing temperature 58 °C), following manufacturer protocol. Each amplicon was, then, purified and analyzed by direct sequencing in a 3500 Genetic Analyzer (Applied Biosystems®, Thermofisher Scientific) using a Big Dye Terminator Cycle sequencing reaction kit (BigDye™ Terminator v3.1 Cycle Sequencing Kit, Applied Biosystems®, Thermofisher Scientific). The resultant sequence data were compared with the updated consensus Cambridge sequence (GenBank accession number: NC_012920.1). Each sample foresaw 3 replicates.

2.3. Genomic DNA whole exome sequencing

Genomic DNA was extracted by peripheral blood of all family members and purified by the QIAamp DNA Blood Mini Kit (Qiagen). Quali-quantitative assessment was, then, performed by Qubit fluorometer (Thermo Fisher Scientific). Paired-end libraries were generated by the SureSelect XT HS Reagent Kit (V7-Post) (Agilent) kit and sequenced on a NovaSeq 6000 Illumina platform. All samples foresaw 3 replicates. Produced raw data were quality checked by the FastQC (v.0.12.1) tool (http://www.bioinformatics.babraham.ac.uk/projects/fastqc) and filtered according to Phred score value (reads with Phred score <30 were trimmed, along with adaptor sequences). Then, the trimmed reads were aligned with precision to the Human Reference Genome (GRCh38/hg38) using Novocraft NovoAlign v.4.03.08 (https://www.novocraft.com/products/novoalign/), followed by the application of the Genome Analysis Toolkit version 4 (GATK4, https://gatk.broadinstitute.org/) for variant calling, with standard setup. Concurrently, sequencing data was processed through the CLC Genomics Workbench v.24.0.0 (https://digitalinsights.qiagen.com/). The analytical protocol commenced with stringent read alignment to GRCh38, permitting ≤3 mismatches/100bp, followed by duplicate removal, InDel realignment, and BQSR. Variant detection utilized Fixed Ploidy calling, accepting variants with posterior probability >90 % and excluding pyrosequencing artifacts via specific filters (homopolymer regions ≥3 nucleotides; variant frequency <0.8). Subsequently, an integrative step was undertaken to merge the overlapping data derived from the Novoalign-GATK4 and CLC Genomics Workbench analytical pathways. This critical phase involved a meticulous comparison and validation process, ensuring the concordance of variant calls between the two platforms. The merging was executed with stringent criteria for variant quality scores and read depth, ensuring that only the most reliable and substantiated variants were carried forward for downstream analysis. This rigorous, dual-platform approach provided a robust framework for the identification of both common and rare variants, offering a comprehensive genomic landscape. The resultant dataset, a harmonized compilation of high-confidence variants, stood ready for subsequent phases of functional annotation and pathogenicity assessment by ANNOVAR v.20231125 tool and included databases [23].

2.4. Filtering and Sanger validation of gDNA candidate variants

The initial phase of candidate variant selection involved scrutinizing newly identified variants for prior associations with Cone-rod dystrophy (CORD) or other Inherited Retinal Diseases (IRDs), leveraging a comprehensive set of reference databases integrated within

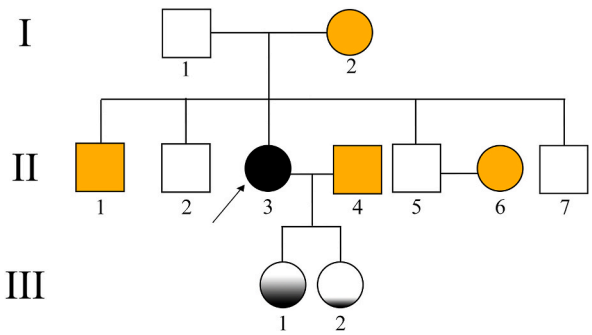

Fig. 1. Pedigree of the Sicilian family affected by a suspected orphan form of MIDD. The affected (black fill) and unaffected (no fill) members are shown. Yellow fill indicates symptomatology potentially related only to specific aspect of main pathological phenotype (e.g. diabetes). Gradient black fill denotes the variable expression of the proband's phenotype. More details through the text. Arrow: proband; circle: female; square: male.

ANNOVAR, including ClinVar, the Complete Genomics datasets (cg46 and cg69), the NHLBI-ESP project datasets (esp6500siv2), ExAC databases, dbSNP, the gene4denovo201907 database, gnomAD collections, Kaviar database, Haplotype Reference Consortium data, ABraOM, several datasets from the 1000 Genomes Project (ranging from 2010 to 2015) and HapMap. This was complemented by data from HGMD Professional (https://digitalinsights.qiagen.com/), Leiden Open Variation Database (LOVD) v.3.0 (https://www.lovd.nl/), and the RetNet database (https://web.sph.uth.edu/RetNet/), providing a robust foundation for frequency and association analysis. Subsequently, an in-depth functional impact assessment of the variants was conducted, focusing on: 1) Variants within coding regions; 2) Variants implicated in potential splice site modifications; 3) Regulatory variants located in 3′ and 5' untranslated regions (UTRs); 4) Variants exhibiting high sequence conservation across species. A comparison of selected variants between all analyzed exomes was also realized. Variants filtered in family affected members were validated by Sanger sequencing. Primers were designed by Primer3 tool [24], following standard settings and, then, carefully manually checked. Then the performed protocol was the same already described in section 2.2 for the m.3243A > G. Primer list and PCR thermal conditions are available upon request.

2.5. Mitochondrial DNA whole genome sequencing

Genomic DNA (gDNA) was initially evaluated for integrity via agarose gel electrophoresis and quantified using the Quant-IT PicoGreen assay (Invitrogen). For amplicon generation, 10 ng of gDNA underwent PCR amplification to produce two long PCR amplicons, 9.1 kb and 11.2 kb in size, covering the entire human mitochondrial DNA (mtDNA) genome. The PCR utilized primers MTL-F1 (5- AAA GCA CAT ACC AAG GCC AC -3), MTL-R1 (5- TTG GCT CTC CTT GCA AAG TT -3), MTL-F2 (5- TAT CCG CCA TCC CAT ACA TT -3), and MTL-R2 (5- AAT GTT GAG CCG TAG ATG CC -3). Post-amplification, amplicon quantification was performed using Quant-IT PicoGreen (Invitrogen), and quality assessment was conducted using the Bioanalyzer 12000 DNA chip (Agilent Technologies). For library construction, 2 ng of each PCR amplicon was pooled and prepared using the Nextera XT DNA Sample Preparation Kit, adhering to the manufacturer's instructions. The final libraries were quantified via qPCR as per the KAPA Library Quantification Kits for Illumina Sequencing platforms and quality-checked using the Agilent Technologies 2200 TapeStation. Raw data generation was executed on the Illumina NovaSeq 6000 Platform, which produced raw images and base calling through the integrated primary analysis software RTA (Real-Time Analysis). The BCL/cBCL (base calls) binary files were converted into FASTQ format using the Illumina package bcl2fastq2-v2.20.0, with the demultiplexing option (–barcode-mismatches) set to ensure a perfect match (value: 0). This meticulous process ensures the production of high-quality, reliable sequencing data for comprehensive analysis and interpretation of mitochondrial DNA. Each sample foresaw 3 replicates. Post-acquisition, mtDNA raw data were rigorously validated and analyzed for variant calling using the Hadoop-based mtDNA-Server, tailored for mtDNA NGS data processing [25]. HadoopBAM partitioned input data, retaining only high-quality reads (Phred score >20, length >25 nucleotides) and discarding duplicates. The server tallied quality-passed bases per strand (A, C, G, T, N, d) at each genomic site. Heteroplasmy detection involved filtering sites with low coverage (<10 bases per strand) and excluding mitochondrial hotspots (positions 309, 315, 3107). Sites with allele coverage ≥3 bp per strand and VAF ≥1 % underwent a machine learning model analysis, considering sequencing errors per strand. Sites with LLR ≥5 were marked as heteroplasmic, with heteroplasmy levels calculated as a weighted mean from both strands. The mtDNA-Server also performed intra-sample contamination checks to prevent misinterpretations, especially in cases of mtDNA sequence disparities. It generated VAF-based profiles for minor (VAF <50 %) and major (VAF >50 %) components, leading to the identification of distinct, valid haplogroups, thus ensuring the mtDNA analysis's integrity and reliability.

2.6. Annotating, prioritizing, and predicting in silico mtDNA Variant Consequences

In our mtDNA WGS methodology, we meticulously adhered to key principles to ensure the accuracy and relevance of variant analysis. This included a focus on low heteroplasmy levels, evaluating variant frequencies in the general population and specific haplogroups, analyzing data for clinical penetrance modulation, and considering inter-species nucleotide/amino acid conservation. MITOHPC was employed to assess mitochondrial health, analyzing indicators like DNA copy number, mutation load, and heteroplasmy levels [26]. MITY (https://github.com/KCCG/mity) was utilized for detailed annotation and interpretation of mtDNA variants, employing a comprehensive variant database and predictive algorithms to classify mutations and provide annotations on protein function, haplogroup context, and evolutionary conservation. MITOMAP served as a reference for known mtDNA mutations, offering information on disease associations and population frequencies. MITOMASTER facilitated sequence alignment, variant identification, and haplogroup determination against the revised Cambridge Reference Sequence (rCRS), enhancing the analysis of mtDNA structure and variation [27]. For variant analysis, we used mvTool from the MSeqDR infrastructure to support mtDNA nomenclatures, annotate novel variants, and provide updated population data and pathogenic classifications [28]. Unannotated variants underwent analysis using the Ensembl Variant Effect Predictor (VEP), and precise mtDNA haplogroup assignment was performed using the PhyMer sub-tool. To refine our annotations, we employed MITOS2 [29], which uses BLAST searches and previously annotated protein sequences to detect protein-coding genes, tRNAs, and rRNA, ensuring accurate genome annotation. Tools like Mitomap and MToolBox [30] were instrumental in understanding variant prevalence and heteroplasmic fractions, aligning reconstructed contigs against macro-haplogroup-specific consensus sequences for private variant detection and clinical investigation. This process also involved considering the pathogenicity of each mutated allele, nucleotide variability, and amino acid variability for codogenic variant sites. Finally, to complete the variant data, we integrated insights from the MitoBreak database, focusing on mtDNA rearrangements, including breakpoints from linear mtDNAs, deletions, and duplications [31]. In our approach to mtDNA NGS, we navigated the complexity of novel variants of unknown significance (VUS) by leveraging a suite of in-silico prediction tools. These tools, focusing on interspecies sequence conservation and structural analysis, helped assess the functional impact of variants. Key among these was

MitImpact 3D v.3.1.2, offering pre-computed pathogenicity prediction scores for non-synonymous substitutions in mitochondrial protein-coding genes [32]. We utilized an array of missense pathogenicity predictors and meta-predictors from MitImpact 3D, including SIFT, PolyPhen2, MutationAssessor, and others, each providing nuanced insights into variant pathogenicity. These were complemented by evolutionary conservation indices like PhyloP and PhastCons, and site-specific variability assessments like SiteVar and MISTIC Mutual Information scores. MitImpact 3D also facilitated the evaluation of compensated pathogenic deviations (CPDs) and significant intra-protein covariations using EV Mutation and I-COMS. Further enriching our analysis, HmtVAR provided a comprehensive repository of variability and pathogenicity data for human mtDNA variants, integrating records from various databases and in-house assessments [33]. It offered curated tRNA variant attributes, while specialized resources like MITOTIP and PON-mt-tRNA delivered predictions based on secondary structure information, structural analogies, conservation scores, and multifactorial scores associating various features, enhancing the specificity and sensitivity of our variant interpretation [34].

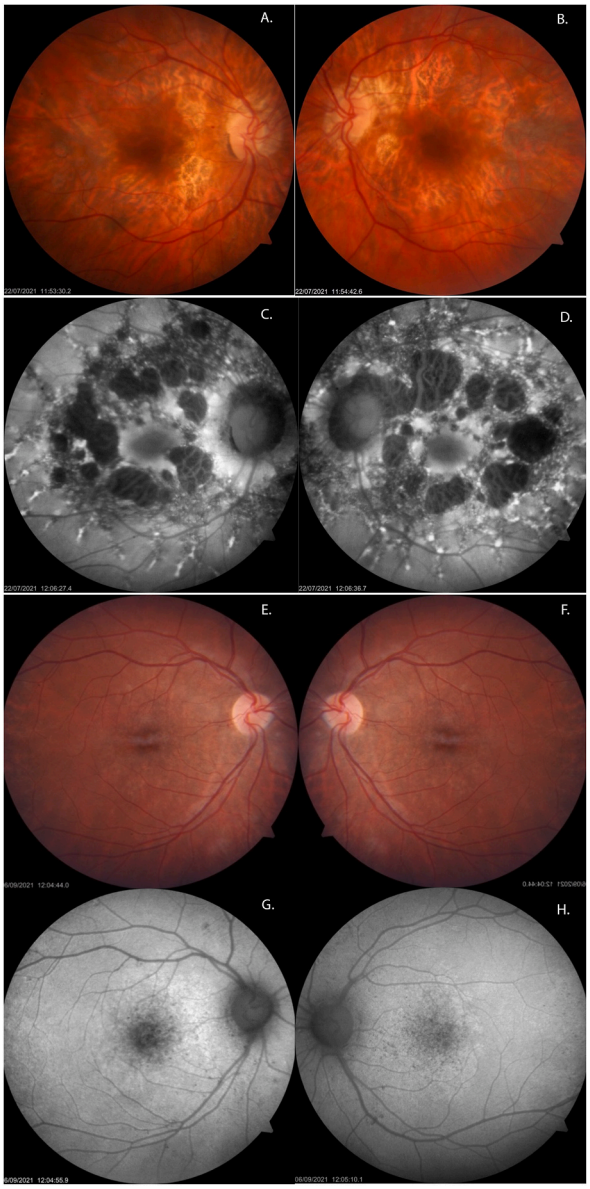

Fig. 2. Color fundus and autofluorescence of proband and her youngest daughter**.** Proband's color fundus showed retinal pigment epithelium atrophy at the posterior pole encircling the macular region **(**A. Left eye. B. Right Eye). Proband's fundus autofluorescence highlights hyperpigmented areas show increased autofluorescence, whereas hypopigmented spots exhibit decreased in autofluorescence, corresponding to chorioretinal atrophy; adjacent to the temporal vascular arcade speckled AF patterns surrounding areas of atrophy. (C. Left eye. D. Right Eye). E-H panels show the youngest daughter's color fundus (E. Left eye. F. Right Eye) and fundus autofluorescence (G. Left eye. H. Right Eye).

Table 1

Identified Genetic Variants in Genes Associated with Retinal Homeostasis and Mitochondrial Function in the Family with MIDD. The table summarizes the identified single nucleotide polymorphisms (SNPs) and new mutations across 17 genes implicated in retinal homeostasis and mitochondrial activities across the analyzed family. The table provides information on the gene, its protein function, the specific SNP or mutation, the consequence of the variant, the variant allele, the minor allele frequency (MAF), associated diseases or syndromes (if applicable), and the genotypes for the proband (II3), the proband's husband (II4), and their two daughters (III1 and III2).

GENE	PROTEIN FUNCTION	SNP	CONSEQUENCE	VARIANT	MAF	HGMD	II3	II4	III1	III2
AHNAK2	Ca^{2+} Signalling	rs775973653	Synonymous	T > C	<0.01		+/−	+/+	+/−	+/+
		c.11305, p.Val3769Met	Missense	G > A	?		+/−	+/+	+/−	+/+
		rs10438246	Missense	T > C	0.44		−/−	+/+	−/−	−/−
		rs371085059	Missense	G > C	<0.01		+/−	+/+	+/−	−/−
		rs761643215	Synonymous	T > C	<0.01		+/−	+/+	+/−	−/−
		rs199891797	Missense	G > T	<0.01		+/−	+/+	+/−	−/−
		rs1454134952	Missense	G > C	<0.01		+/−	+/+	+/−	−/−
		rs1292576510	Synonymous	A > G	<0.01		+/−	+/+	+/−	−/−
		rs369661152	Missense	T > A	<0.01		+/−	+/+	+/−	−/−
		rs761745272	Synonymous	G > C	<0.01		−/−	+/+	+/−	+/+
		rs1595395121	Missense	G > A	<0.01		+/−	+/+	+/+	+/+
		rs530346059	Missense	A > G	<0.01		+/−	+/+	+/−	−/−
		rs538732616	Missense	G > A	<0.01		−/−	+/+	+/−	−/−
		rs552547151	Missense	G > C	<0.01		+/−	+/+	+/−	−/−
		rs767950030	Missense	A > G	<0.01		+/−	+/+	+/+	+/+
		rs569119829	Missense	T > C	<0.01		+/−	+/+	+/−	+/+
		rs1898124035	Synonymous	G > C	<0.01		+/−	+/+	+/+	+/+
		rs770786113	Synonymous	A > C	<0.01		+/−	+/+	+/−	+/+
		rs1399215160	Synonymous	C > T	<0.01		+/−	+/+	+/+	+/+
		rs537844199	Synonymous	A > G	<0.01		+/−	+/+	+/+	+/+
		rs554470062	Synonymous	T > C	0.02		+/−	+/+	+/−	−/−
		rs1258653775	Synonymous	C > T	<0.01		+/−	+/+	+/−	+/+
		rs201817721	Synonymous	T > C	0.06		+/−	+/+	+/−	−/−
		rs1303676939	Missense	C > T	<0.01		+/−	+/+	+/−	+/+
		rs757916382	Missense	A > G	<0.01		+/−	+/+	+/−	−/−
		rs11160825	Missense	C > T	0.45		+/−	+/+	+/−	−/−
		rs773366246	Synonymous	C > T	<0.01		+/−	+/+	+/−	+/+
		rs777095278	Missense	T > C	<0.01		+/−	+/+	+/−	+/+
		rs751108438	Synonymous	T > C	<0.01		+/−	+/+	+/−	−/−
		rs781323817	Missense	T > C	<0.01		+/−	+/+	+/−	+/+
		rs199536215	Missense	T > C	<0.01		+/−	+/+	+/−	−/−
		rs748258992	Synonymous	G > A	<0.01		+/−	+/+	+/−	+/+
		c.11385, p.Asp3795Asp	Synonymous	T > C	?		+/−	+/+	+/−	+/+
		c.11639, p.Ala3880Val	Missense	C > T	?		−/−	+/+	+/−	+/+
		rs760792869	Synonymous	T > C	<0.01		+/−	+/+	+/−	+/+
		c.11972, p.Glu3880Gly	Missense	G > T	?		+/−	+/+	+/−	+/+
		rs199717476	Missense	C > T	<0.01		+/−	+/+	+/−	−/−
		rs1197255416	Synonymous	C > G	<0.01		+/−	+/+	+/+	+/+
		rs1253609445	Synonymous	A > G	<0.01		+/−	+/+	+/−	−/−
		rs762470858	Missense	G > A	<0.01		+/−	+/+	+/−	−/−
ALDH3A2	Detoxification of aldehydes generated by alcohol metabolism and lipid peroxidation	rs141112437	Missense	T > C	0		+/−	+/+	+/+	+/−
ALMS1	Microtubule organization and maintenance of cilia	c.105_110, p.Ala35_Asn36insLysLys	Inframe Insertion	INS GGAGGA	?		+/−	+/+	+/+	+/+

(*continued on next page*)

Table 1 (*continued*)

GENE	PROTEIN FUNCTION	SNP	CONSEQUENCE	VARIANT	MAF	HGMD	II3	II4	III1	III2
CAPN5	Signal transduction, Ca^{2+}-dependent cysteine protease, regulates cell mechanics, presynaptic depolarization and opening of Ca^{2+} channels	rs2233546	Missense	C > T	0.04		+/−	+/+	+/+	+/−
COQ4	Coenzyme Q; involved in the electron transport chain	c.202_203insA	3′ UTR	INS A	?		−/−	−/−	−/−	−/−
		rs3003601	Missense	G > C	<0.01	Neonatal encephalomyopathy-cardiomyopathy-respiratory distress syndrome	−/−	−/−	−/−	−/−
DDX21	RNA helicase; linked to process involving RNA second structure as nuclear and mitochondrial splicing	rs376034982	5′ UTR	C > T	<0.01		+/−	+/−	+/+	+/−
		rs5030896	Intron	A > G	0.05		−/−	−/−	−/−	−/−
EP400	ATP-dependent chromatin remodeler activity, H2A and H4 acetylation	rs7974276	Missense	A > G	0.29		+/−	+/−	+/−	−/−
		rs1555223313	Inframe Insertion	INS GCA	?		−/−	+/−	+/−	−/−
ERCC2	DNA Repair	rs757790912	Stop Gained	G > C	<0.01	Xerodema Pigmentosum	+/−	+/+	+/+	+/+
		rs1799793	Missense	C > T	0.19	Cerebrooculofacioskeletal Syndrome 2, Trichothiodystrophy 1 Photosensitive, Xeroderma Pigmentosum	+/−	+/−	+/−	−/−
		rs755174338	Missense	C > T	<0.01	Xerodema Pigmentosum	+/−	+/+	+/−	+/−
KIR2DL1	Transmembrane glycoproteins for regulation of the immune response	rs762460075	Inframe Deletion	DEL CTT	<0.01		+/+	+/+	+/−	+/+
		rs368954426	Missense	G > A	<0.01		+/+	+/+	+/−	+/+
		rs1234293357	Missense	T > C	<0.01		+/+	+/+	+/−	+/+
		rs532526797	Synonymous	C > T	0.02		+/+	+/+	+/−	+/+
		rs10414159	Synonymous	A > G	0.12		+/+	+/+	+/−	+/+
		rs595008	Synonymous	A > C	<0.01		+/+	+/+	+/−	+/+
KIR2DL3		rs756958902	Missense	A > G	<0.01		+/−	+/−	+/−	+/−
		rs111321678	3′ UTR	C > G	0.02		+/−	+/−	+/−	+/−
		rs528067108	3′ UTR	G > A	<0.01		+/−	+/−	+/−	+/−
		rs1159242166	3′ UTR	T > C	<0.01		+/−	+/−	+/−	+/−
		rs683216	3′ UTR	T > A	0.05		+/−	+/−	+/−	+/−
		rs200347365	Synonymous	C > T	0.30		+/−	+/−	+/−	+/+
LRRK2	Associated with the mitochondrial outer membrane; regulates intracellular and synaptic vesicles	rs751144618	Intron	T > C	<0.01		/	/	+/−	+/−
		rs200827521	Missense	C > T	<0.01		+/+	+/+	+/+	+/−
MKKS	Centrosome-shuttling protein, role in cytokinesis, interacts with BBSome for ciliary membrane biogenesis	rs137853909	Missense	T > C	<0.01	Bardet-Biedl Syndrome	+/−	+/+	+/−	+/−
MTA3	Histone deacetylase binding activity, transcription co-activator or co-repressor	rs1670563971	Missense	G > T	<0.01		+/−	+/+	+/−	+/−
MTOR	Cellular metabolism regulator, stress signals, response to hormones, circadian rhythms	rs139043855	Missense	C > T	<0.01	Isolated Focal Cortical Dysplasia Type II	+/−	+/+	+/+	+/−
PER3	Involved in circadian rhythms by transcriptional regulation	rs228701	Intron	A > G	0.30		+/−	−/−	+/−	−/−
		c.2947_3001del GCTCTG TCCACA GGATCGCCT CCCATGAAGA ATCCATCCCA TCCTACTGCCAGC	Del	DEL GCTCTG TCCACA GGATCGCCT CCCATGAAGA ATCCATCCCA TCCTACTGCCAGC	?		+/−	−/−	+/−	−/−

(*continued on next page*)

Table 1 (*continued*)

GENE	PROTEIN FUNCTION	SNP	CONSEQUENCE	VARIANT	MAF	HGMD	II3	II4	III1	III2
POLRMT	mtDNA RNA Polymerase for mtDNA transcription	rs2285855	Intron	G > C	0.50		+/−	−/−	+/−	−/−
POTEJ	Involved in Retinal homeostasis; located in nucleus and extracellular exosomes	rs749185867	Missense	C > G	<0.01		+/−	+/−	+/−	+/−
		rs1229580654	Synonymous	T > C	<0.01		+/−	+/−	+/−	+/−
		rs372122037	Synonymous	C > T	<0.01		+/−	+/−	+/−	+/−
		rs777642649	Synonymous	G > A	<0.01		+/−	+/−	+/−	+/−
		rs913248209	Missense	A > G	<0.01		+/−	+/−	+/−	+/−
		c.2138, p.Lys713Ile	Missense	A > T	?		+/−	+/−	+/−	+/−
		c.2157, p.Lys719Asn	Missense	G > T	?		+/−	+/−	+/−	+/−
RP1L1	Regulate microtubule polymerization, affecting photosensitivity and outer segment morphogenesis	c.4032, p.Thr1344Ala	Missense	T > C	?		+/−	+/+	+/+	+/−
		rs1461300678	Missense	C > T	<0.01		+/−	+/+	+/+	+/−
		rs141205444	Missense	T > A	0.17		+/−	+/+	+/−	+/+
SPHK2	In mitochondria, cytochrome c-oxidase assembly and mitochondrial respiration of rods. In nucleus, epigenetic regulation of gene expression	rs769831160	Missense	C > G	<0.01		+/−	+/−	+/−	+/−
		rs145253804	Missense	G > T	<0.01		+/−	+/+	+/−	+/−
		rs1485196478	Synonymous	T > C	<0.01		+/−	+/−	+/−	+/−
STAT2	Nucleus transcription activator, regulates mitochondrial fission	rs1356843849	Missense	G > C	<0.01	Primary immunodeficiency with post-measies-mumps-rubella vaccine viral infection	+/−	+/+	+/+	+/+
		rs2229363	Missense	C > A	<0.01	Primary immunodeficiency with post-measies-mumps-rubella vaccine viral infection	+/−	+/+/	+/−	+/−
TEFM	Increases mtRNA polymerase processivity, regulates transcription of mtDNA, including genes important for the oxidative phosphorilation	c.289, p.Glu97Gln	Missense	C > G	?		+/−	+/+	+/+	+/−
TENT5A	Enables RNA binding activity and it is involved in mRNA stabilization	rs3186631	Synonymous	A > G	0.12		+/−	+/+	+/−	+/+
		rs1303194940	Missense	C > A	<0.01		+/−	+/+	+/−	+/+
TRMT61B	Involved in mitochondrial mRNA and tRNA methylation	rs139225663	Missense	C > A	<0.01		+/−	+/+	+/−	+/−
USH2A	In photoreceptors, it is required for the maintenance of periciliary membrane complex involved in regulating intracellular protein transport	rs77211159	Missense	C > T	0.02	Usher Syndrome 2a	+/−	+/+	+/+	+/−
		rs41315587	Missense	C > T	0.04	Usher Syndrome 2a	+/−	+/+	+/+	+/−
		rs41304083	Synonymous	G > A	0.04	Usher Syndrome 2a	+/−	+/+	+/+	+/−
		rs76137174	Intron	T > C	0.02		+/−	+/+	+/+	+/−
WDPCP	Effector of the planar cell polarity signalling pathway which regulates the septin cytoskeleton in both ciliogenesis and collective cell movements	rs769165669	Missense	G > A	<0.01	Bardet-Biedl Syndrome	+/−	+/+	+/−	+/−

2.7. Whole genome bisulfite sequencing of both gDNA and mtDNA

For WGBS library preparation, DNA from each family member (40 ng) was amalgamated with 4 pg of unmethylated lambda DNA (Promega, #D1521, Madison, WI, USA) and 4 pg of CpG methylated puc19 DNA (NEB, #E7120S, Ipswich, MA, USA), serving as spike-in controls. Fragmentation of the DNA was carried out to achieve an average size of 350 bp utilizing the Covaris E220 system (Covaris, Woburn, MA, USA). Subsequent to fragmentation, the DNA underwent bisulfite treatment, meticulously following the protocol provided with the EZ DNA Methylation-Gold Kit (Zymo, #D5005, Irvine, CA, USA). Post-treatment, DNA purification was performed using Zymo-Spin™ IC Columns, after which it was processed for library construction utilizing the Accel-NGS Methyl-Seq DNA Library kit. To ascertain the integrity and concentration of the library, a 4200 TapeStation system (Agilent, Santa Clara, CA, USA) was employed, complemented by quantitative analysis with a KAPA library quantification kit (Roche #07960336001, Basel, Switzerland). The sequencing was executed on an Illumina Novaseq 6000 S1 flow cell, achieving 150 bp paired-end reads. This included a strategic 30 % spike-in of whole-genome sequencing libraries to enrich the dataset. To ensure adequate depth and quality, each sample was thrice replicated.

2.8. Whole genome bisulfite sequencing (WGBS) data-processing pipeline

In WGBS data analysis, the methodology started with alignment and methylation calling, predominantly facilitated by Bismark aligner, integrated in the Msuite 2.2.0, a comprehensive and streamlined tool for WGBS data analysis [35]. It integrates alignment, methylation calling, and DMR (Differentially Methylated Region) detection into a unified workflow. Msuite begins with the alignment of bisulfite-treated reads using Bismark and, then, obtained BAM files underwent sorting, indexing for deduplication, and bias plot verification. Next, the methylation calling was followed by an optimized DMR detection algorithm that considers the spatial distribution of methylation and the biological variance across samples. To improve the strength of down-stream data, the Bismark output was integrated with CLC Genomics Workbench 24.0.0 data analyses, then followed by a parallel pipeline with other specialized tools. The first was related to methylation extraction, pivotal for discerning methylation patterns, which employed MethylDackel 0.5.2 (https://github.com/dpryan79/MethylDackel). This stage involves read-genome comparison, decoding methylation statuses, and addressing biases in read extraction. MethylDackel's output, the bedGraph file, encapsulates methylation data per position, serving as a substrate for subsequent data filtration and analysis. The next phase, data normalization and statistical analysis, focuses on CpG methylation. Given the absence of a standardized normalization method for sequence data and the impact of library preparation methods on CpG coverage, downsampling is employed to normalize read sequence counts at the extraction level, preserving methylation call integrity, CpG site read count distribution, and coverage accuracy. The culmination of this process is the detection of DMRs, involving comprehensive analysis of genomic regions across samples. The quest for DMRs, a cornerstone in understanding epigenetic mechanisms, involves a sophisticated array of statistical tools and methodologies, each meticulously tailored with specific parameters to enhance detection accuracy. BSmooth introduces a local likelihood smoothing approach, paired with Welch's *t*-test, to discern methylation variations across samples, setting precise P-value thresholds to delineate DMRs [36]. BiSeq 1.42.0 addresses potential type II errors through a beta-binomial model, integrating a false discovery rate and refining detection via a hierarchical, triangular kernel model (https://bioconductor.org/packages/release/bioc/html/BiSeq.html). MethylSig 1.14.0 and Metilene 0.2.8, utilizing the beta-binomial model, add depth to the analysis – MethylSig by considering read coverage and biological variance [37], and Metilene through binary segmentation and multivariate Kolmogorov-Smirnov tests, sensitively attuning to sample distribution differences [38]. methylKit 1.28.0 brings to the table Fisher's exact test and logistical regression-based statistics, adeptly adjusting P-values with the Benjamini-Hochberg method, resonating with the binomial nature of methylation scores [39]. Defiant 1.1.9, a standalone tool, employs weighted Welch expansion and Fisher's exact test or Welch's *t*-test based on the sample set, meticulously weighting sample variance based on coverage. This suite of tools, each with its unique approach and finely tuned parameters, ensures not just the precision of DMR detection but also encapsulates the complexity and variability inherent in biological data and epigenetic landscapes [40]. DMRich 1.7.1, on the other hand, is a specialized tool designed for the high-resolution identification of DMRs. It employs a sliding-window approach, coupled with a sophisticated statistical framework, to detect regions with significant methylation differences. DMRich's algorithm accounts for coverage depth and biological variability. Its robust statistical model ensures the accurate pinpointing of DMRs, even in datasets with complex epigenetic patterns [41].

2.9. Pathway analyses of differentialy methylated and mutated gDNA and mtDNA genes

To finally hypothesize the molecular mechanisms at the basis of the possible MIDD orphan form affecting the family, the GO term enrichment analysis for differentially methylated and mutated gDNA and mtDNA genes was performed using the ClueGO (v. 2.5.10) (INSERM, Paris, France) [42] and CluePedia (v. 1.5.10) (INSERM, Paris, France) [43] plugins in Cytoscape (ver. 3.10.1) (National Institute of General Medical Sciences, Bethesda, MD, USA) [44]. The configuration for ClueGO was meticulously established as follows: the ontologies chosen encompassed CLINVAR, GO (spanning Biological Process, Cellular Component, Molecular Function, and Immune System Process), INTERPRO, KEGG, REACTOME (inclusive of Pathways and Reactions), WIKIPATHWAYS, and CORUM 3.0. The hierarchy levels for the GO Tree were precisely defined, with the minimum level set at 2 and the maximum at 9. Criteria for the selection of GO Terms/Pathways were rigorously applied, requiring a minimum of 2 genes and a minimum percentage of 3 % genes. The network connectivity threshold, determined by the Kappa Score, was fixed at 0.4. Statistical parameters were stringently set to perform Enrichment/Depletion analysis using the Two-Sided hypergeometric test, with p-value correction implemented via the Bonferroni step-down method. CluePedia was engaged with its default parameters. In the final selection phase, only GO terms manifesting a

P-value less than 0.01 were considered.

2.10. Validation of gDNA and mtDNA methylation by pyrosequencing

Pyrosequencing technology was employed to acquire quantifiable data on DNA methylation [16]. Initially, 500 ng of genomic DNA underwent sodium bisulfite conversion using the EZ DNA Methylation™ Kit (Zymo Research), adhering strictly to the protocol provided by the manufacturer. The PCR composition included 20 ng of sodium bisulfite-converted DNA, 1x PyroMark PCR master mix (QIAGEN, Hilden, Germany), 1x CoralLoad Concentrate (QIAGEN, Hilden, Germany), and 200 nM of each respective primer, culminating in a total volume of 25 μl. The PCR procedure commenced with a 15-min denaturation phase at 95 °C, succeeded by 45 cycles each comprising 30 s at 95 °C, 30 s at 58 °C, and 30 s at 72 °C. A final elongation phase was conducted for 10 min at 72 °C. The sequences for the primers are available upon request.

3. Results

3.1. Clinical analysis of family members evidenced a maternally inherited diabetes and deafness phenotype in the proband

The Sicilian family showed a mitochondrial inheritance pattern, with the proband (II3) which probably transmitted the most of phenotype characters to the daughters (Fig. 1). The proband was affected by type II diabetes and arterial hypertension, and complained visual disturbances since the age of 35 years, she used to wear glasses, but visual loss worsened in the last two years; not nyctalopia or visual field or color vision defect. She was mild deaf. She presented in the right eye best corrected visual acuity of 20/100 and 20/32 in the left eye, clear lenses, intraocular pressure in the normal range and a patchy atrophy at the fundus examination with macular sparing (Fig. 2A–B), confirmed with macular OCT scans and FA: in FAF multifocal and multinodular well demarcated hypoautofluorescence areas from the absence of retinal pigment epithelium (RPE), surrounded by mottled hyperautofluorescence areas. Such lesions were distributed in the posterior pole of the retina and in the peripapillary region: more anteriorly, at the level of the principal temporal vascular arcades, multiple linear hyperfluorescence stripes characterized the RPE dystrophy (Fig. 2, C-D).

All the instrumental exams on proband's eyes converged to MIDD retinal alteration comorbidity.

The oldest daughter was affected by deaf-mutism and high myopia and did not show specific other ocular condition; her best corrected visual acuity was 20/35 in both the eyes. The youngest was affected by thyroid dysfunction under treatment, her best corrected visual acuity was 20/20 and at the fundus examination she showed a mild maculopathy characterized by hard drusen and irregular patchy RPE atrophy at the posterior pole, while FAF showed patchy hyper and hypoautofluorescence at the posterior pole and in mid periphery (Fig. 2, E-H). She was unaware of her condition, and she did not complain any visual disturbances.

The husband showed a mild form of type II diabetes and glaucoma. His best correct visual acuity was 20/20 in both the eyes and anterior segment and posterior segment were unremarkable.

Finally, clinical analyses evidenced a maternally inherited diabetes and deafness phenotype in the proband.

3.2. The comprehensive WES analysis revealed a complex genetic landscape of MIDD associated with variants in nuclear genes involved in retinal homeostasis, mitochondrial function, and epigenetic regulation

Sequencing run of all samples outputted a mean of 100 million reads. About 94 % of total reads showed a Phred score >30. Around 43,000 variants were detected for each sample. Statistics of the sequencing run are available upon request, while complete variant calling results are presented in Table S1. Found variants were, then, filtered as described in the methods section, and upon detailed examination of the genetic landscape within the family, our study revealed a complex interplay of genetic variants that correlate with the disease's clinical manifestations. In the comprehensive genomic analysis of our study subjects, a total of 61 SNPs and 7 new mutations were identified and filtered across 17 genes implicated in retinal homeostasis and mitochondrial activities. The proband (II3), diagnosed with MIDD, carries a series of rare variants with minor allele frequencies (MAF) less than 0.01 in genes such as *AHNAK2*, *EP400*, *ERCC2*, *KIR2DL1*, *KIR2DL3*, *POTEJ*, *RP1L1*, *SPHK2*, and *WDPCP*, which were also shared with the likely affected daughter (III1). These variants include 19 missense and coding sequence mutations in *AHNAK2*, a stop-gained mutation in ERCC2 (rs757790912, G > C), as well as deleterious mutations in *KIR2DL1* (rs762460075, DEL CTT; rs368954426, G > A; rs1234293357, T > C), *KIR2DL3* (rs756958902, A > G), *POTEJ* (rs913248209, A > G), *RP1L1* (rs1461300678, C > T), and *WDPCP* (rs769165669, G > A), suggesting a potential significant role in the pathogenesis of MIDD. Contrastingly, the healthy husband (II4) and daughter (III2) displayed a markedly different genetic profile, with fewer of these critical variants, highlighting the potential protective genomic landscape against MIDD. Notably, the presence of variants with a higher MAF, such as rs10438246 in *AHNAK2* (T > C, MAF = 0.44), among all family members, underscores the genetic diversity and suggests that not all shared variants contribute to the disease phenotype. Additionally, the analysis revealed several other notable variants in genes associated with various cellular processes relevant to MIDD pathophysiology. The proband and the likely affected daughter carried variants in *ALMS1* (new Inframe insertion INS GGAGGA), *MTOR* (rs139043855, C > T), and *TEFM* (new missense C > G), which are involved in microtubule organization, cellular metabolism regulation, and mitochondrial transcription, respectively. Furthermore, variants in genes like *ALDH3A2* (rs141112437, T > C), *CAPN5* (rs2233546, C > T), *COQ4* (new 3′ UTR INS A; rs3003601, G > C), *DDX21* (rs376034982, C > T), *MTA3* (rs1670563971, G > T), *STAT2* (rs1356843849, G > C; rs2229363, C > A), and *TRMT61B* (rs139225663, C > A) suggest potential disruptions in detoxification pathways, signal transduction, electron transport chain, RNA splicing, chromatin remodeling, transcriptional regulation, and mitochondrial RNA modification. More details in Table 1.

3.3. A deeper pathway analysis of molecular mechanisms and candidate therapeutic targets through available databases and machine learning approaches highlighted important implications of epigenetic regulation in MIDD etiopathogenesis

The comprehensive analysis of the intricate network of diseases, biological functions, and canonical pathways has revealed critical insights into the multifaceted nature of disease mechanisms and potential therapeutic targets. By employing advanced machine learning techniques, we have delineated a broad spectrum of conditions ranging from Endocrine System Disorders and Neurological Diseases to Hereditary Disorders, as illustrated in Fig. 3A. These findings highlight the complex interplay between genetic predispositions and cellular processes. The analysis underscores the significance of Cellular Assembly and Organization, Inflammatory Diseases and Responses, and alterations in Cell Morphology and Post-Translational Modifications in understanding the molecular underpinnings of disease states (Fig. 3B). Notably, our findings point to the pivotal role of inflammation in disease progression across various conditions, including Ophthalmic Diseases, and emphasize the intricate balance between Cellular Movement, Lipid Metabolism, and Small Molecule Biochemistry in the maintenance of cellular and metabolic homeostasis. Among the canonical pathways identified (Fig. 3C), the Pyroptosis Signaling Pathway, PI3K/AKT Signaling, and DNA Double-Strand Break Repair by Homologous Recombination stand out not only for their direct implications in disease mechanisms but also for their potential involvement in epigenetic regulation processes. These pathways suggest a layer of complexity where epigenetic modifications could influence gene expression and cellular responses, thereby modulating disease progression and response to therapy. Furthermore, the investigation into canonical pathways such as Phagosome Formation, Caveolar-mediated Endocytosis Signaling, and the critical role of the

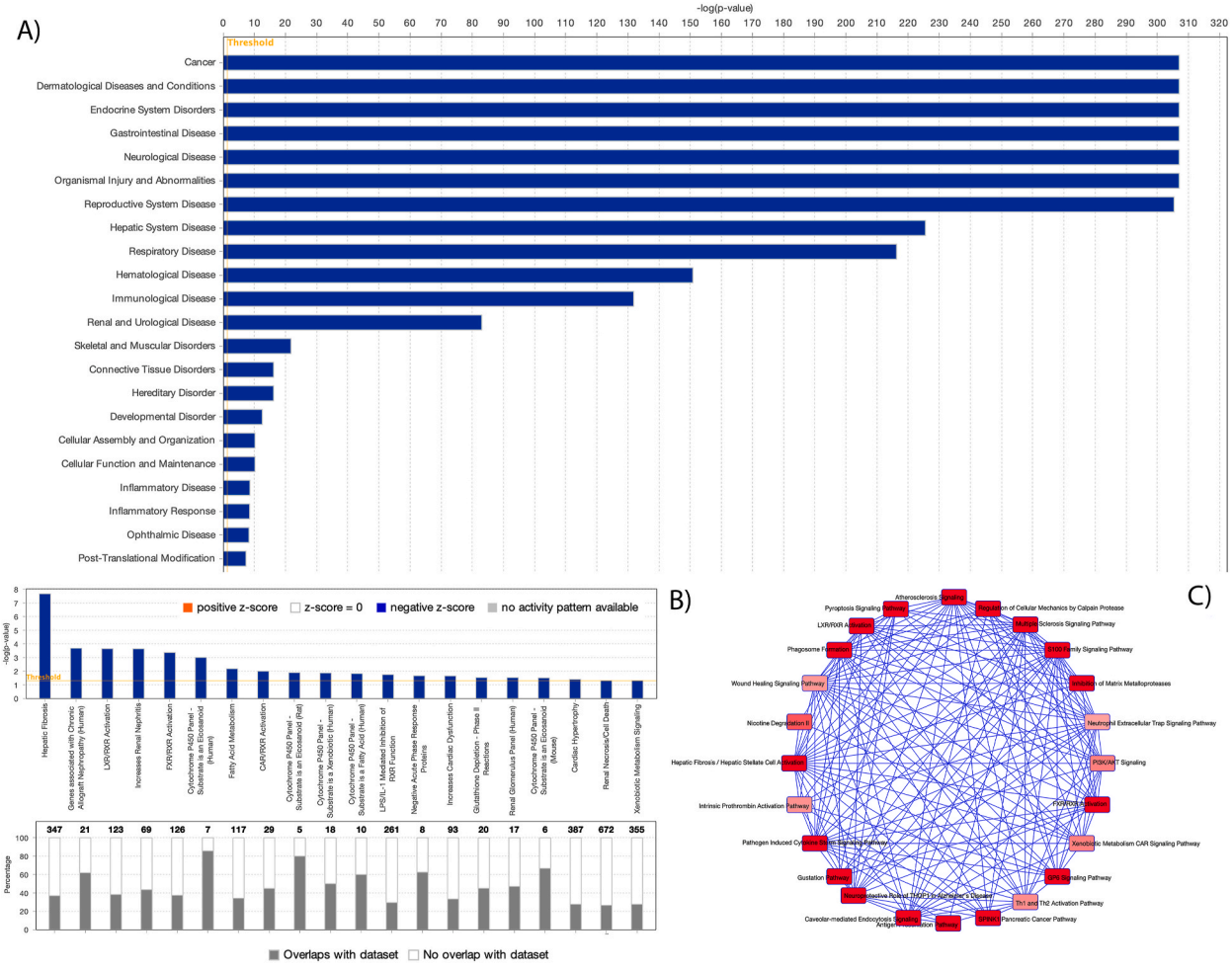

Fig. 3. Multidimensional analysis of WGS genotypic variations and phenotypic expressions. These figures collectively contribute to a deeper understanding of the complex interplay between genetic variations and their phenotypic outcomes in the context of MIDD. Panel A delineates the Interesting Diseases and Bio-Functions, spotlighting crucial biological processes and disease states significantly associated with our dataset, underscoring their potential impact and relevance. Panel B details the Tox List, identifying specific toxicological responses and pathways activated in response to chemical exposures or environmental stressors, offering insights into the toxicogenomic profile of our dataset. Panel C illustrates Overlapping Canonical Pathways, capturing the intersection of significantly enriched pathways across different conditions or datasets, highlighting shared molecular mechanisms.

Glucocorticoid Receptor Signaling pathway (Fig. 4) reveals essential cellular uptake, processing mechanisms, and survival pathways fundamental to disease development and progression. Moreover, the focus on DNA repair mechanisms and stress response pathways (Fig. 5) highlights their critical roles in maintaining cellular integrity, with epigenetic regulation playing a key role in fine-tuning these processes. A novel aspect of our study is the identification of specific disease pathways through machine learning, including Familial Diabetes Mellitus, Hereditary Retinal Diseases, and various forms of Macular and Retinal Dystrophy (Fig. 3A). These pathways not only shed light on the genetic and mitochondrial disorders affecting the eye but also underscore the potential of machine learning in revealing novel disease mechanisms and therapeutic targets, including those influenced by epigenetic modifications.

3.4. In-depth analysis of mtDNA variants and their heteroplasmy level enforced the hypothesis that mtDNA represents the pivotal regulator of MIDD molecular mechanisms

The sequencing run for all samples yielded an average of 120 million reads, with approximately 91 % of the total reads exhibiting a Phred score greater than 30. The deep study of mtDNA through the study subjects has unveiled a rich tapestry of genetic variation across multiple genes and loci, coupled with a spectrum of heteroplasmy levels that underscore the complexity of mitochondrial genetics (Table 2). The gene *MT-ND5* emerged as a significant hotspot with 11 distinct variants, indicating a potential focal point for mutation within the mitochondrial genome. This was closely followed by other genes such as *MT-ATP8*, *MT-RNR1*, *MT-ATP6*, and *MT-CYB*, each contributing to the diversity with multiple variants. Particularly notable were the variants m.263A > G in *MT-HV2* and m.709G > A in *MT-RNR1*, showcasing high heteroplasmy levels of 99.83 % and 99.94 %, respectively. These levels suggest a pronounced prevalence of these mutations within the mtDNA of the affected cells, pointing towards their potential significance in the mitochondrial genetic landscape. The discovery of a nearly homoplasmic insertion, m.310_320insCTCCCCCGCT in *MT-HV2*, with a heteroplasmy level of 99.97 %, adds a new dimension to our understanding, potentially serving as a biomarker for MIDD. Conversely, variants like the m.523_526delCCG in *MT-HV3*, with a heteroplasmy level of only 1.37 %, illustrate the variability in the presence of certain mutations within the mtDNA, which may contribute to phenotypic diversity. The analysis further categorized mtDNA variants by mutation type, with transitions being predominant, followed by an insertion, a deletion, and a transversion, primarily located in non-coding regions crucial for mitochondrial replication and transcription regulation. The average heteroplasmy level across all analyzed variants was approximately 44.06 %, reflecting a broad spectrum of variant prevalence. This variation in heteroplasmy levels, from as low as 1.01 % to as high as 99.97 %, suggests varying degrees of penetrance and potentially diverse impacts on mitochondrial function. Sequence conservation analysis, as indicated by global sequence counts and frequencies, revealed interesting patterns. For instance, the m.263A > G transition was found to be exceptionally frequent in the general population, showcasing a frequency of 95.527 % in FL and 57.217 % in CR databases, highlighting its potential ubiquity. In contrast, other transitions, like the m.709G > A, exhibited lower commonality, with specific frequencies suggesting a narrower distribution. All identified mtDNA variants are carried by both the Proband (II3) and daughter (III1).

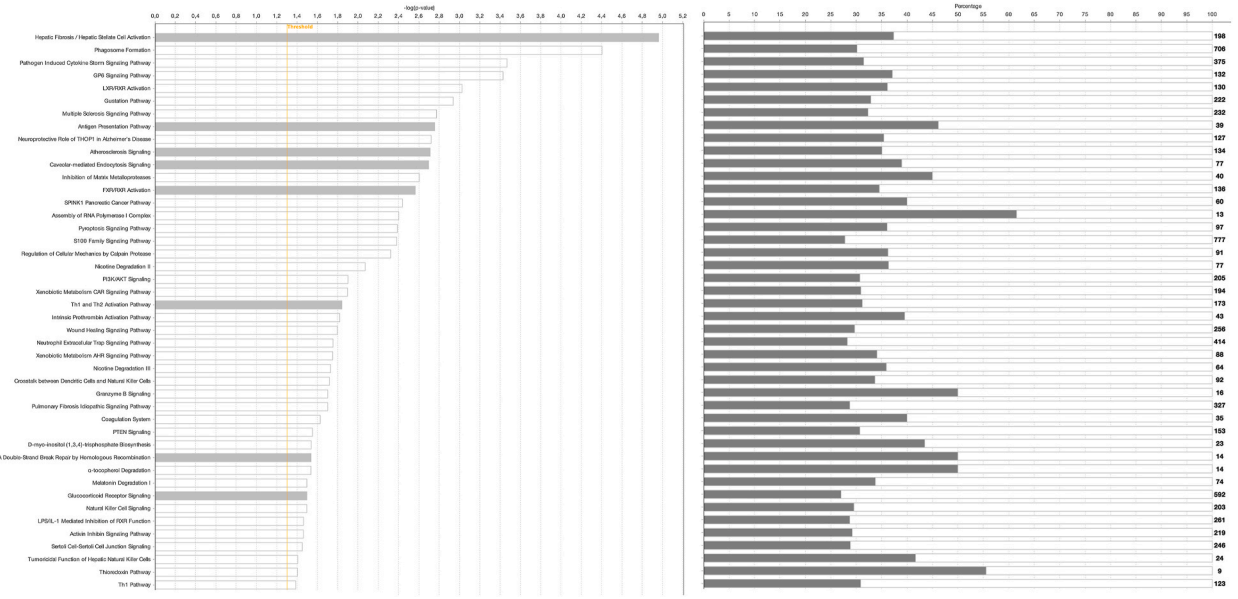

Fig. 4. Analysis of Pathway Enrichment in Mitochondrial Diabetes: Prioritizing Biological Impact through Canonical Pathways. These figures collectively contribute to a deeper understanding of the complex interplay between genetic variations and their phenotypic outcomes in the context of MIDD. Panel D presents a Canonical Pathways Vertical Stacked Bar Chart, quantitatively summarizing the -log(p-value) of enriched pathways to prioritize those most significantly affected, providing a clear hierarchy of biological impact.

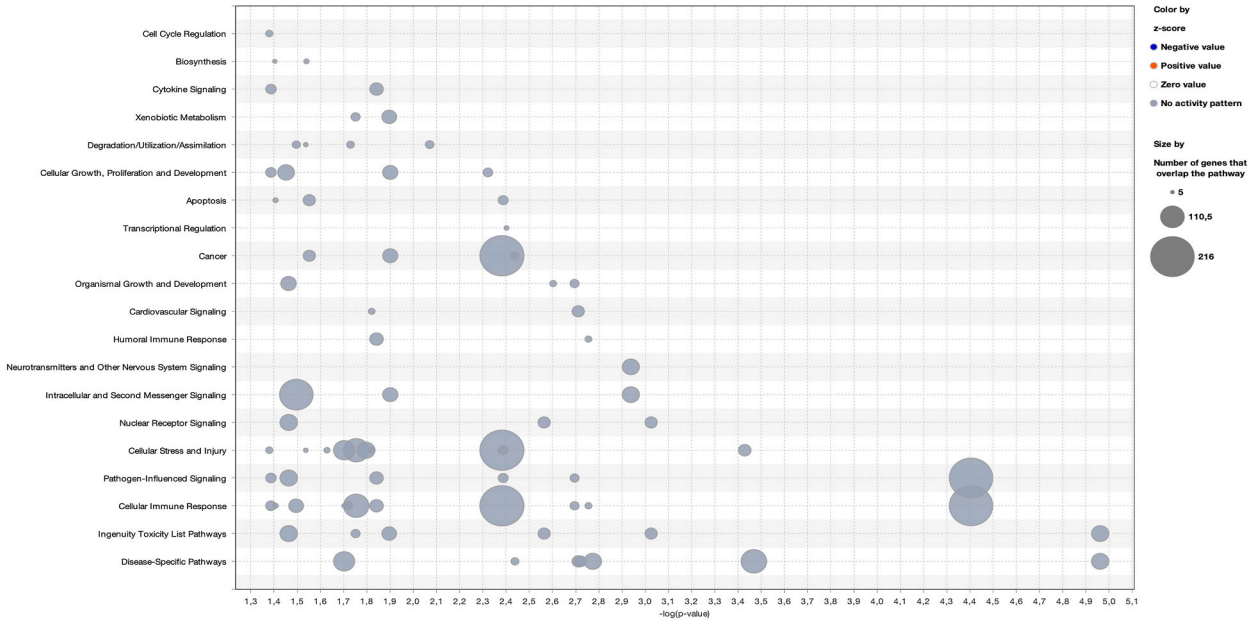

Fig. 5. Visualizing Pathway Enrichment in Mitochondrial Diabetes: Insights from a Canonical Pathways Bubble Chart. These figures collectively contribute to a deeper understanding of the complex interplay between genetic variations and their phenotypic outcomes in the context of MIDD. Lastly, Panel E showcases a Canonical Pathways Bubble Chart, where the size and color of each bubble represent the significance and the ratio of dataset genes involved in each pathway, respectively, offering a visually intuitive understanding of pathway enrichment and relevance.

3.5. Alteration of different mitochondrial biochemical pathways could lead to MIDD onset and evolution

The pathway analyses of mtDNA mutated genes carried by the family members delineated a complex interplay among genetic predispositions, metabolic dysfunctions, and cellular derangements underpinning a spectrum of symptoms, including hereditary, metabolic, neurological, ophthalmic, and endocrine disorders, alongside pronounced inflammatory responses. Notably, our dataset elucidation underscored the paramount significance of mitochondrial bioenergetics, with oxidative phosphorylation and mitochondrial dysfunction emerging as critical nodes within the pathophysiological landscape. Predominantly, our findings accentuated mitochondrial bioenergetics, with oxidative phosphorylation and mitochondrial dysfunction emerging as critical nodes within the pathophysiological landscape. This emphasis on mitochondrial pathways underscores the organelle's pivotal role in cellular energetics and survival, positing mitochondrial dysfunction as a nexus for diverse pathological states. Such insights suggest that therapeutic modalities aimed at restoring mitochondrial function could exert wide-ranging effects across multiple disease entities. Moreover, the application of machine learning techniques to our disease pathway analysis revealed a pronounced focus on mitochondrial DNA-related disorders, affirming the hypothesis that mitochondrial genetic anomalies contribute significantly to the observed disease phenotypes. This revelation not only corroborates the centrality of mitochondrial genetics in disease etiology but also opens novel investigative corridors for elucidating the genetic mechanisms underlying mitochondrial pathologies. Further, the analysis of canonical pathways illuminated critical regulatory mechanisms, notably nuclear receptor signaling, cellular stress and injury responses, and transcriptional regulation pathways. The involvement of nuclear receptor signaling pathways highlights the intricate balance between hormonal regulation and disease manifestation, suggesting potential for targeted intervention through modulation of these pathways. Additionally, the identification of cellular stress and injury, along with transcriptional regulation pathways, underscores the cellular adaptive mechanisms to both exogenous and endogenous stressors, highlighting the criticality of maintaining cellular homeostasis and the fidelity of gene expression regulation in disease prevention and progression. The convergence of data on overlapping canonical pathways, including mTOR signaling, eIF4 and p70S6K signaling, and viral pathogenesis, offers insight into the shared molecular mechanisms undergirding diverse pathological conditions, suggesting a commonality in the biological processes disrupted across diseases. Such findings not only provide a unifying thematic framework for understanding disease pathology but also spotlight potential targets for interventions with broad-spectrum therapeutic efficacy. Further details are available in Fig. 6

3.6. The epigenomic landscape analyses evidenced relevant methylation patterns across mutated nuclear genes within the family genomes

The sequencing effort across all samples generated an average output of 630 million reads, where roughly 91 % of these reads achieved a Phred score exceeding 30 (see Fig. 7). About 346,000 DMRs were found throughout the entire genome comparison between the proband and the healthy husband (Table S2). The methylation pattern of the proband is the same in the probably affected daughter, while the other daughter exhibited a pattern similar to the father. Integrating the comprehensive insights from our genomic analysis, we weave a narrative that delves deep into the subtleties of epigenetic modifications against the backdrop of the genomic landscape's

Table 2

Mitochondrial DNA Variants Identified in the Family with MIDD. The table summarizes the mitochondrial mtDNA variants identified across the family. The table provides information on the start and end positions of the variants, the HGVS (Human Genome Variation Society) notation, the gene or locus affected, the gene or locus description, the variant heteroplasmy, the alternate depth (ALT_DEPTH), the reference depth (REF_DEPTH), the total sample depth (TOTAL_SAMPLE_DEPTH), the total locus depth (TOTAL_LOCUS_DEPTH), the mutation type, the locus, other annotations, the frequency of the variant in various databases (GBSEQSCOUNT, FREQ), the number of references supporting the variant (REFS), and the conservation score across species (CONSERVATION).

HGVS	GENE/ LOCUS	GENE/LOCUS DESCRIPTION	VARIANT HETEROPLASMY	ALT DEPTH	REF DEPTH	TOTAL SAMPLE DEPTH	TOTAL LOCUS DEPTH	LOCUS	OTHER	GB SEQSCOUNT (FREQ)*‡	CONS.
m.263A > G	MT-HV2	Hypervariable segment 2 [classic:73–340]; H-strand origins; 7S DNA. D-Loop, involved in DNA topology, DNA recombination, mtDNA replication, membrane association, dNTP metabolism	0,9983	295528	491	296019	296019	CR:HVS2CR: OHATTCR: Control Region	non-coding	FL:58432 (95.527 %) CR:45942 (57.217 %)	NA
m.310_320insCTCCCCCGCT	MT-HV2	Hypervariable segment 2; H-strand origins; Conserved sequence block 2; 7S DNA D-Loop, involved in DNA topology, DNA recombination, mtDNA replication, membrane association, dNTP metabolism	0,9997	134861	37	134898	134898	CR:HVS2CR: OHCR: CSB2ATTCR: Control Region	non-coding	FL:0 (0.000 %) CR:0 (0.000 %)	NA
m.523_526delCCG	MT-HV3	Hypervariable segment 3; membrane attachment site; 7S DNA D-Loop, involved in DNA topology, DNA recombination, mtDNA replication, membrane association, dNTP metabolism	0,0137	4176	299802	303978	303978	CR:HVS3CR: Control Region	non-coding	FL:0 (0.000 %) CR:0 (0.000 %)	NA
m.539T > A	MT-HV3	Hypervariable segment 3; mtTF1 binding site; membrane attachment site; 7S DNA D-Loop, involved in DNA topology, DNA recombination, mtDNA replication, membrane association, dNTP metabolism	0,0108	4784	440064	444848	444848	CR:HVS3CR: TFHCR:Control Region	non-coding	FL:0 (0.000 %) CR:3 (0.004 %)	NA
m.709G > A	MT-RNR1	Mt_rRNA → Enables DNA binding activity and DNA-binding transcription factor binding activity; involved in several processes, including regulation of carbohydrate utilization and phosphate metabolic processes.	0,9994	1610416	1025	1611441	1611441	12S	rRNA	FL:7994 (13.069 %) CR:0 (0.000 %)	40 %
m.750A > G	MT-RNR1		0,9994	1647139	1031	1648170	1648170	12S	rRNA	FL:60122 (98.290 %) CR:0 (0.000 %)	98 %
m.1008A > G	MT-RNR1		0,9979	2015370	4152	2019522	2019522	12S	rRNA	FL:36 (0.059 %)CR:0 (0.000 %)	60 %
m.2259C > T	MT-RNR2		0,9982	1096288	1935	1098223	1098223	16S	rRNA	FL:320 (0.523 %)CR:0 (0.000 %)	33 %
m.3599T > C	MT-ND1	Protein_coding → Located in mitochondrial membrane; enables ubiquinone activity and	0,0101	1822	178938	180760	180760	ND2	frameshift	FL:0 (0.000 %) CR:0 (0.000 %)	A:60.00 % A:13.33 % T:53.33 %

(*continued on next page*)

Table 2 (*continued*)

HGVS	GENE/ LOCUS	GENE/LOCUS DESCRIPTION	VARIANT HETEROPLASMY	ALT DEPTH	REF DEPTH	TOTAL SAMPLE DEPTH	TOTAL LOCUS DEPTH	LOCUS	OTHER	GB SEQSCOUNT (FREQ)*‡	CONS.
		be involved I mitochondrial electron transport									A:91.11 % A:95.56 %
m.4611_4614delATAA	MT-ND2		0,0123	6363	511953	518316	518316	ND2	ND2: M100 M	FL:59732 (97.652 %) CR:0 (0.000 %)	24 %
m.4769A > G	MT-ND2		0,999	395267	413	395680	395680	COII	COII: L160V	FL:0 (0.000 %) CR:0 (0.000 %)	96 %
m.8063T > G	MT-CO2	Protein_coding → Located in mitochondrial inner membrane and involved in cytochrome *c* to oxygen electron transport	0,012	6214	510672	516886	516886	COII	COII: P189P	FL:901 (1.473 %)CR:0 (0.000 %)	100 %
m.8152G > A	MT-CO2		0,9955	738925	3314	742239	742239	ATPase8	ATPase8: L20L	FL:0 (0.000 %) CR:0 (0.000 %)	89 %
m.8425A > C	MT-ATP8	Protein_coding → Involved in mitochondrial ATP synthesis coupled proton transport	0,0131	5901	444244	450145	450145	ATPase8	ATPase8: Y33S	FL:0 (0.000 %) CR:0 (0.000 %)	53 %
m.8463A > C	MT-ATP8		0,0138	6656	474095	480751	480751	ATPase8	ATPase8: H34P	FL:0 (0.000 %) CR:0 (0.000 %)	22 %
m.8466A > C	MT-ATP8		0,0123	6049	484026	490075	490075	ATPase8	ATPase8: L35L	FL:1 (0.002 %) CR:0 (0.000 %)	16 %
m.8470A > C	MT-ATP8		0,0209	9026	423815	432841	432841	ATPase6	ATPase6: L25L	FL:0 (0.000 %) CR:0 (0.000 %)	40 %
m.8601A > C	MT-ATP6		0,0154	6646	424133	430779	430779	ATPase6	ATPase6: T112A	FL:60264 (98.522 %) CR:0 (0.000 %)	71 %
m.8860A > G	MT-ATP6		0,9975	625720	1568	627288	627288	ATPase6	ATPase6: M140T	FL:19 (0.031 %)CR:0 (0.000 %)	87 %
m.8945T > C	MT-ATP6		0,9996	903432	371	903803	903803	COIII	COIII: P123P	FL:419 (0.685 %)CR:0 (0.000 %)	96 %
m.9575G > A	MT-CO3	Protein_coding → Located in mitochondrial inner membrane and involved in cytochrome *c* to oxygen electron transport	0,9981	417535	806	418341	418341	ND4	ND4: L441L	FL:0 (0.000 %) CR:0 (0.000 %)	49 %
m.12082A > C	MT-ND4	Protein_coding → Located in mitochondrial membrane; enables ubiquinone activity and be involved I mitochondrial electron transport	0,0126	13466	1051085	1064551	1064551	ND5	frameshift	FL:0 (0.000 %) CR:0 (0.000 %)	A:28.89 % A:17.78 % C:60.00 % T:82.22 % C:40.00 %
m.12425_12428delACTC	MT-ND5		0,0332	31568	919596	951164	951164	ND5	ND5: N109S	FL:83 (0.136 %)CR:0 (0.000 %)	9 %
m.12662A > G	MT-ND5		0,9986	864897	1249	866146	866146	ND5	ND5: I257V	FL:4134 (6.758 %)CR:0 (0.000 %)	44 %
m.13105A > G	MT-ND5		0,9994	557446	329	557775	557775	ND5	ND5: N470H	FL:0 (0.000 %) CR:0 (0.000 %)	53 %
m.13744A > C	MT-ND5		0,0152	2363	152965	155328	155328	ND5	ND5: I472L	FL:0 (0.000 %) CR:0 (0.000 %)	78 %

(*continued on next page*)

Table 2 (*continued*)

HGVS	GENE/ LOCUS	GENE/LOCUS DESCRIPTION	VARIANT HETEROPLASMY	ALT DEPTH	REF DEPTH	TOTAL SAMPLE DEPTH	TOTAL LOCUS DEPTH	LOCUS	OTHER	GB SEQSCOUNT (FREQ)*‡	CONS.
m.13750A > C	MT-ND5		0,0124	1802	143211	145013	145013	ND5	ND5: A475A	FL:0 (0.000 %) CR:0 (0.000 %)	2 %
m.13761A > C	MT-ND5		0,0242	1404	56529	57933	57933	ND5	ND5: S476A	FL:47 (0.077 %)CR:0 (0.000 %)	29 %
m.13762T > G	MT-ND5		0,0305	2169	68958	71127	71127	ND5	ND5: F478V	FL:0 (0.000 %) CR:0 (0.000 %)	2 %
m.13768T > G	MT-ND5		0,0131	1077	81270	82347	82347	ND5	ND5: L484R	FL:0 (0.000 %) CR:0 (0.000 %)	36 %
m.13787T > G	MT-ND5		0,0113	1345	118003	119348	119348	ND5	ND5: I571L	FL:0 (0.000 %) CR:0 (0.000 %)	16 %
m.14047A > C	MT-ND5		0,0105	3239	305923	309162	309162	ND5	ND5: T573P	FL:0 (0.000 %) CR:0 (0.000 %)	13 %
m.14053A > C	MT-ND5		0,0148	5024	334695	339719	339719	Cytb	Cytb:I42I	FL:373 (0.610 %)CR:0 (0.000 %)	71 %
m.14872C > T	MT-CYB	Protein_coding → Enable metal ion binding activity; involved in electron transport coupled proton transport, response to cobalamin, response to glucagon	0,999	848317	869	849186	849186	Cytb	Cytb: T194A	FL:60315 (98.605 %) CR:0 (0.000 %)	18 %
m.15326A > G	MT-CYB		0,9985	1758170	2725	1760895	1760895	Cytb	Cytb: I211L	FL:1 (0.002 %) CR:0 (0.000 %)	73 %
m.15377A > C	MT-CYB		0,016	20004	1232091	1252095	1252095	ATTCR:Control RegionCR: HVS1/ HV1CR:7S-like	non-coding	FL:3549 (5.802 %) CR:7073 (8.809 %)	NA
m.16319G > A	MT-HV1	Hypervariable segment 1 [classic:16024–16365] D-Loop, involved in DNA topology, DNA recombination, mtDNA replication, membrane association, dNTP metabolism	0,997	1859788	5566	1865354	1865354	ATTCR:Control RegionCR:7S-like	non-coding	FL:38030 (62.173 %) CR:33864 (42.175 %)	NA

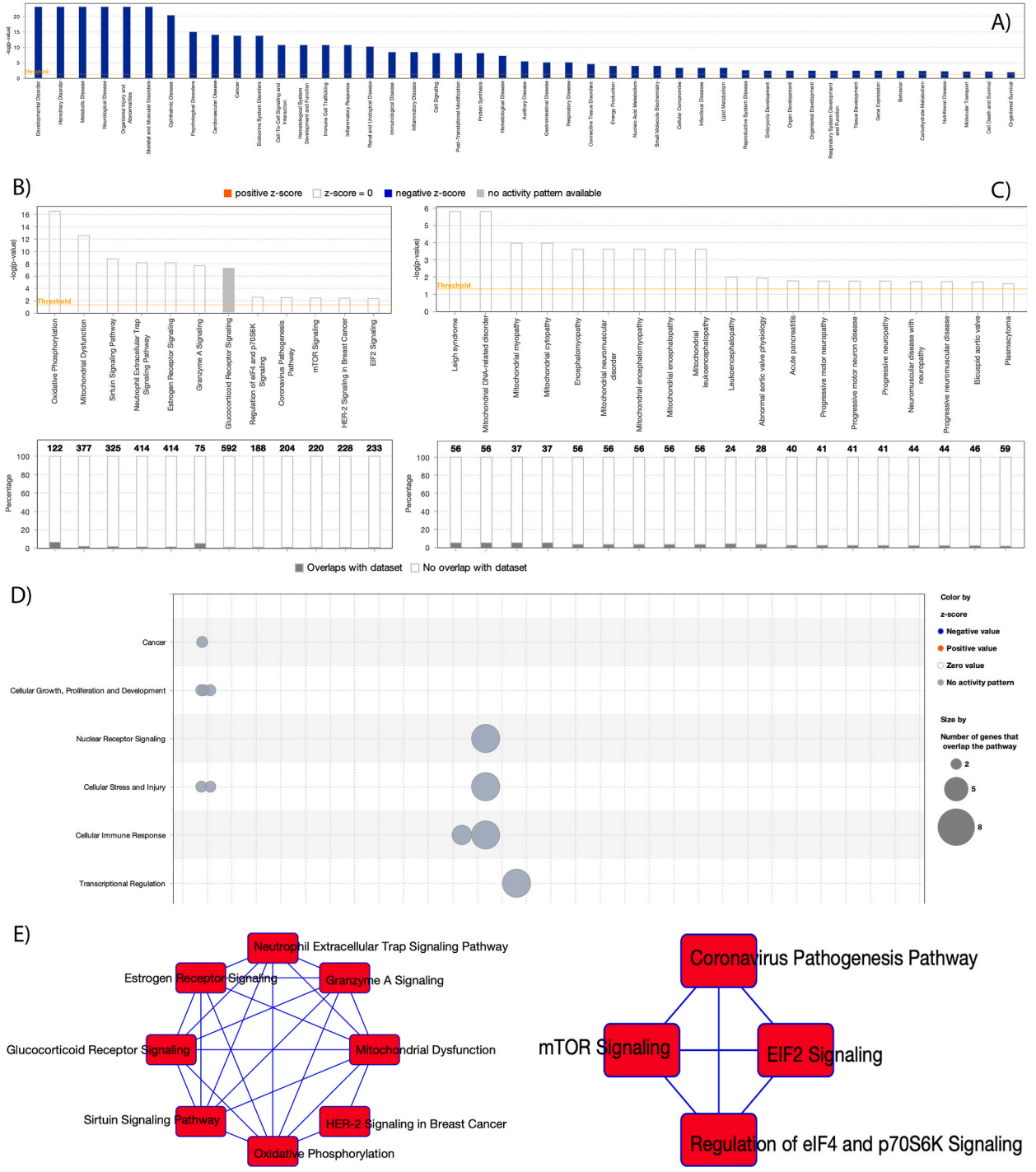

Fig. 6. Integrative Analysis of Molecular Mechanisms related to mtDNA variants. Panel A delineates the spectrum of diseases and bio-functions, including hereditary, metabolic, neurological, and ophthalmic disorders, underlining the genetic and metabolic underpinnings of these conditions. Panel B showcases a vertical stacked bar chart of Canonical Pathways, with oxidative phosphorylation and mitochondrial dysfunction highlighted, emphasizing their critical roles in cellular energetics and disease pathogenesis. Panel C reveals machine-learning-derived disease pathways, focusing on mitochondrial DNA-related disorders, indicating the significant impact of mitochondrial genetics on disease phenotypes. Panel D presents a bubble chart of Canonical Pathways, emphasizing nuclear receptor signaling, cell stress and injury, and transcriptional regulation, illustrating key regulatory mechanisms implicated in disease processes. Panel E illustrates the convergence of overlapping canonical pathways, providing a holistic view of shared molecular mechanisms across diverse pathological states. This figure encapsulates the comprehensive and multifaceted analysis conducted, offering profound insights into the biological basis of disease, with a particular emphasis on mitochondrial function, genetic predispositions, and cellular homeostasis mechanisms.

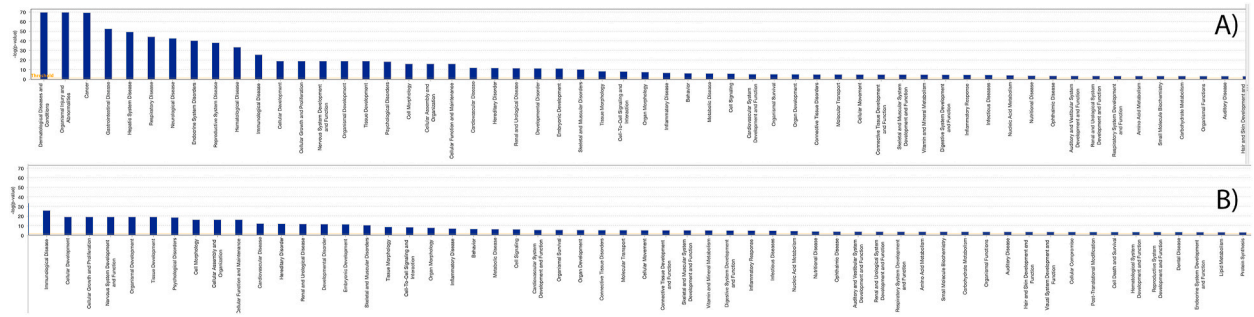

Fig. 7. Unveiling Key Disease Pathways and Biological Functions Through Advanced Molecular Analysis. Panels A and B highlight machine learning-derived disease pathways for ocular conditions, including Syndromic Ciliopathy and Hereditary Eye Diseases.

structural complexity (Table 3). After filtering as stated in Methods section, our study has illuminated profound hypomethylation events, earmarked by a distinct beta coefficient of −0.7058 in the *EYS* gene, signaling significant epigenetic deregulation within territories far removed from traditional regulatory elements like CpG islands, shores, and shelves. This hypomethylation pattern, indicative of a pervasive epigenetic alteration, holds potential ramifications for genomic stability and gene expression regulation across various loci. The *EYS* locus emerged as a hallmark of hypomethylation, showcasing a dramatic beta coefficient that underscores considerable epigenetic deregulation across multiple regions, including exons, introns, and the 3′ UTR. Conversely, *SETBP1* stands as the counterpoint, representing the most hypermethylated gene within our dataset, with its promoter region's beta coefficient of 1.2699 highlighting a stark contrast in epigenetic state, potentially influencing gene silencing. These loci, with their statistically significant and distinct genomic annotations, underline the diverse roles of methylation in gene regulation—from potential activation to the silencing of gene expression. Our detailed explorations further extend to genes such as *ALMS1*, *WDPCP*, and *PTBP2*, each contributing uniquely to the intricate genomic methylation profile. For instance, *ALMS1* illustrates the complex interplay of methylation across its locus, with both hypermethylated and hypomethylated regions observed in the promoter, 3′ UTR, and other regions. Similarly, *WDPCP* and *PTBP2* have emerged from our dataset as genes undergoing noteworthy epigenetic modifications, with WDPCP exhibiting hypomethylation in exons, introns, and the 3′ UTR, while *PTBP2* shows hypomethylation in exons and the promoter region. The hypermethylated state of *SETBP1* further accentuates the intricate balance of methylation states, emphasizing the nuanced influence of epigenetic modifications across the genome. Most DMRs were observed outside traditional CpG islands (100 %) and within the open sea (100 %), underscoring the significance of non-traditional areas of epigenetic influence. This distribution suggests a paradigm shift in our understanding of epigenetic regulation, where previously overlooked regions now emerge as critical landscapes for gene expression modulation. Our descriptive statistics unveil a rich mosaic of the genomic methylation landscape, with promoter regions (23 %), exons (31 %), introns (15 %), and 3′ UTRs (8 %) representing significant portions of DMRs. This distribution highlights the multifaceted impact of methylation on gene regulation, from transcription initiation to post-transcriptional modifications. Details are available in Table 3, which also reveals that the majority of DMRs are located within distal intergenic regions (23 %), emphasizing the potential influence of methylation on long-range gene regulation.

3.7. WGBS of gDNA revealed differential methylation signatures potentially implicated in ocular and systemic disease pathophysiology

The WGBS of gDNA analysis has provided a comprehensive landscape of molecular dysregulation across a spectrum of diseases, with a pronounced emphasis on genetic aberrations implicated in ocular pathologies such as Syndromic Ciliopathy and Hereditary Retinal Diseases. The elucidation of these pathways, alongside significant bio-functional disturbances in cellular development, neurite outgrowth, synaptogenesis, and nervous system integrity, underscores the potential interplay between genomic sequence variants and epigenetic modifications, particularly nuclear genome methylation. Enriched canonical pathways, including those integral to biosynthesis, growth factor signaling, and cellular stress responses observed, may be intimately regulated by methylation patterns within the nuclear genome. Such regulatory methylation could pivotally influence gene expression profiles and consequent phenotypic outcomes, including the phenotypic manifestations associated with MIDD. The complexity of MIDD, with its characteristic retinal involvement, could be intricately linked to epigenetic alterations, especially considering the tissue-specific expression and methylation signatures known to affect mitochondrial function and energy metabolism. The Fig. 7–12 further highlights the potential role of epigenetic regulation in cellular processes such as microtubule dynamics, migration of cells, and axonal guidance signaling. These pathways are crucial for proper cellular organization, motility, and neuronal connectivity, and their dysregulation may contribute to the pathogenesis of MIDD. The predictive modeling analysis has brought Angiotensinogen (AGT) to the forefront as a regulatory molecule with influence over cell movement and neuropathic pain pathways, indicating that its expression and function might be subject to epigenetic modulation via methylation, impacting cellular dynamics and the pathogenesis of neuropathic pain, a symptom commonly overlooked in MIDD patients.

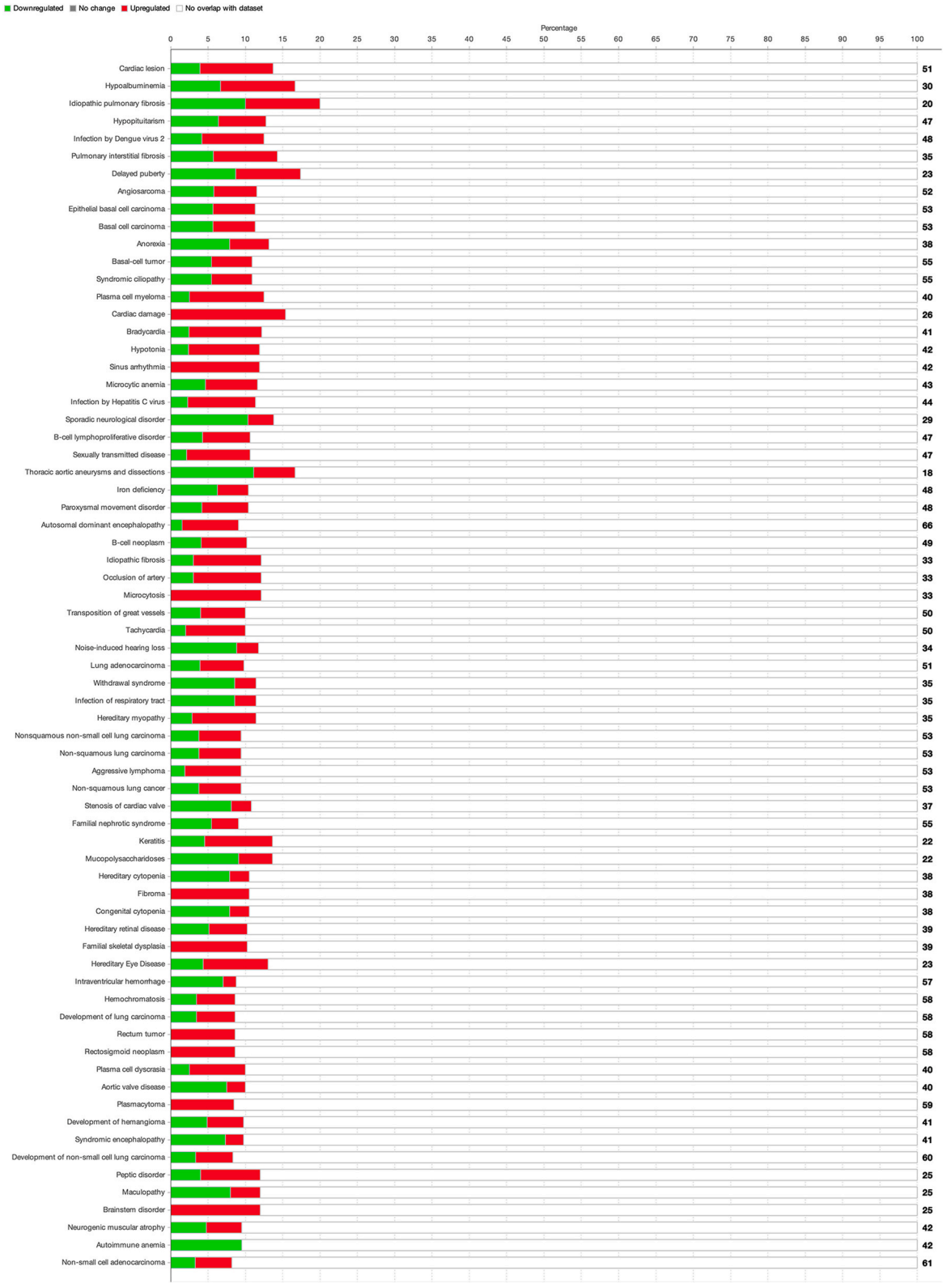

(caption on next page)

Fig. 8. Comparative Analysis of Disease Relevance Across Datasets. This vertical bar chart displays various diseases and conditions, each represented by bars indicating changes or consistencies in data relevance. Red bars signify a downgrade in relevance or inconsistent data, green bars denote an upgrade or positive shift in relevance, and gray bars show no significant change or overlap with the dataset. The percentage scale on the x-axis quantifies these changes, offering insights into the biological impact of these conditions on cellular and metabolic processes.

3.8. Significant shifts in mitochondrial DNA methylation unveiled epigenetic modulations and their impact on gene expression and energy metabolism

After gDNA analyses, the examination of mtDNA methylation patterns suggested significant variations across various mitochondrial regions, unveiling a nuanced landscape of epigenetic modulation within the mitochondrial genome (Table 4). Notably, regions such as MT 1.500 and MT 1001.1500 exhibited marked differences in methylation levels between case and control groups. The former region showed a notable increase in methylation level from 0.0234 (control) to 0.0403 (case), underscored by a Log2 fold change of 0.7858, with a statistically significant p-value of 6.809×10^{-5}. Similarly, the MT 1001.1500 region displayed a change in methylation level from 0.0306 (control) to 0.0461 (case), highlighted by a Log2 fold change of 0.5895, with a p-value of 3.418×10^{-4}. These findings suggest a significant shift in epigenetic regulation within mitochondrial DNA, potentially impacting mitochondrial gene expression and, consequently, mitochondrial function and cellular energy metabolism. Further integrating our detailed insights, we identified key regions, such as MT 501.1000 and MT 10501.11000, that demonstrated pronounced methylation changes between case and control groups, and also stood out for their statistical significance, with p-values reaching as low as 3.474×10^{-10} and 8.018×10^{-10}, respectively. The region spanning MT 501.1000 exhibited the most substantial increase in methylation level, from 0.0213 (control) to 0.0507 (case), marked by a Log2 fold change of 1.2489, suggesting a critical area of epigenetic modulation that could influence mitochondrial gene expression. The region MT 10501.11000 similarly showed a notable increase in methylation level, from 0.0213 (control) to 0.0408 (case), with a Log2 fold change of 0.9361, further underscoring the significant epigenetic alterations within the mitochondrial DNA. The differential methylation patterns observed, particularly in regions proximal to mitochondrial genes such as *MT-RNR1*, *MT-RNR2*, *MT-ND1*, and *MT-ND4L*, underscore the intricate relationship between mitochondrial DNA methylation, gene expression, and mitochondrial functionality. The statistical significance of these changes, reinforced by the detailed analysis of methylation level differences, Log2 fold changes, and p-values, provides compelling evidence of the potential of these epigenetic markers in elucidating the mechanisms underlying mitochondrial function and dysfunction in MIDD (see Fig. 12).

3.9. The impact of mtDNA methylation patterns on the molecular etiology of MIDD might emphasize retinal dysfunction insights

A complex array of bio-functions, with a notable emphasis on Hereditary and Metabolic Disorders, emerged from mtDNA methylation pattern analysis, highlighting the complex interplay between genetic predispositions and metabolic dysregulation (Fig. 13). The pivotal roles of Gene Expression and Protein Synthesis in the manifestation and progression of Ophthalmic Diseases and Endocrine System Disorders underscore the critical importance of cellular mechanisms, such as Cell-to-Cell Signaling and Interaction, alongside Post-translational Modification, for maintaining cellular integrity. The identification of Mitochondrial DNA-related Disorder through machine learning disease pathway analysis corroborates the significant impact of mitochondrial genetics on systemic health. This is particularly relevant in the context of Mitochondrial Dysfunction, which showed a pronounced negative z-score of -2.5 in our Canonical Pathways analysis, suggesting a core underlying mechanism contributing to a wide spectrum of diseases, including the metabolic and auditory phenotypes observed in maternally inherited diabetes and deafness (MIDD), as well as its associated retinal compromise. The recurrence of Mitochondrial Dysfunction across various analysis panels underscores its central role in disease mechanisms, impacting processes ranging from Lipid Metabolism and Small Molecule Biochemistry to Energy Production and Cellular Assembly. This comprehensive identification spans a spectrum of bio-functions impacted by mitochondrial health, suggesting mitochondrial integrity as a linchpin in determining cell fate. Furthermore, the analysis highlights the significance of Free Radical Scavenging, with a positive z-score of 1.5, in combating oxidative stress, a key contributor to mitochondrial and cellular damage, especially pertinent in the retinal dysfunction associated with MIDD. The inclusion of Visual System Development and Function, alongside Nervous System Development, with z-scores of -1.0 and -2.0 respectively, emphasizes the critical impact of mitochondrial function on sensory and neurological health, indicating that aberrations in mtDNA methylation could directly influence the phenotypic manifestations of MIDD, including its retinal aspects. Predictive modeling highlighted Angiotensinogen (AGT) as a regulatory molecule with potential epigenetic modulation via methylation, influencing cellular dynamics and pathogenic pain mechanisms, which could be intricately connected to the broader spectrum of mitochondrial dysfunction's impact on disease pathology. This is supported by the observed dysregulation in pathways related to Cellular Stress and Injury, with a negative z-score of -0.5, and Neuropathic Pain Signaling in Dorsal Horn Neurons, with a z-score of 0.5.

3.10. The gDNA WES and WGBS integrated analysis suggested a tight relationship between nuclear and mitochondrial regulation

The integrated analysis between WES and WGBS gDNA outcomes revealed an extensive epigenetic variability throughout the whole genome (Fig. S1), and especially across the 18 gene loci and 20 kinds of variants potentially associated with MIDD. Several genes exhibited variant-specific DMRs, demonstrating both hypermethylation and hypomethylation compared to the control sample (Fig. 14). Notably, *LRRK2* displayed significant 5′ hypermethylation (log2 fold change 0.79, $p < 0.01$), potentially impacting retinal degeneration in MIDD. *KIR2DL1* and *KIR2DL3* also showed 5′ hypermethylation (log2 fold changes 0.70, $p < 0.001$ and 1.06, $p <$

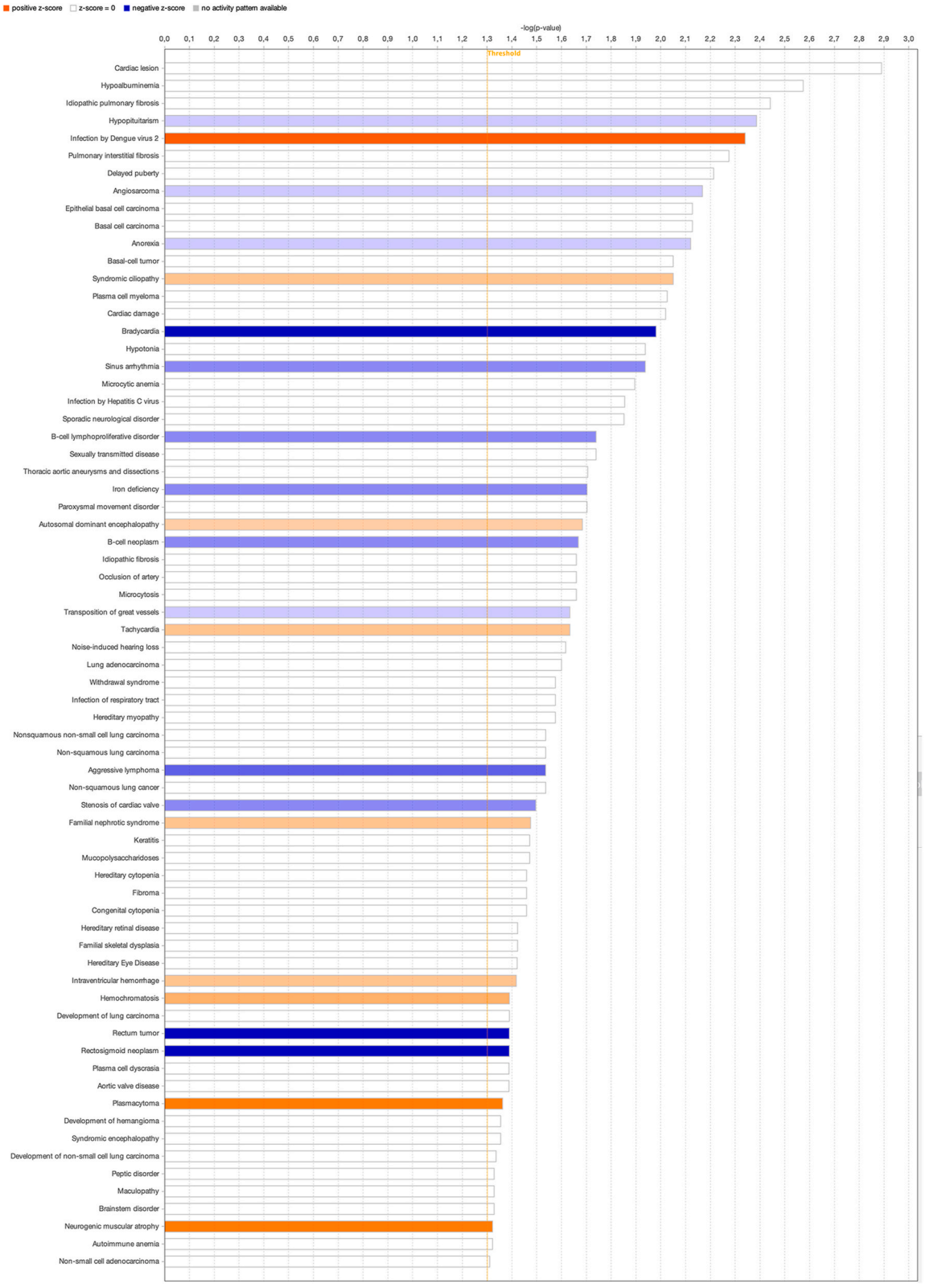

(caption on next page)

Fig. 9. Detailed Pattern Analysis of Disease Relevance. This horizontal bar chart further explores the pattern variability across diseases and conditions as indicated by dataset findings. Bars are colored to represent positive (orange), negative (blue), and inactive (gray) patterns, with their significance reflected through the -log(p-value) on the x-axis. This detailed visualization aids in understanding the significant levels of biological and clinical relevance of the diseases in the dataset.

0.0001), which could disrupt immune surveillance and contribute to diabetic retinopathy. *SPHK2* exhibited 3′ hypomethylation (log2 fold change −1.25, $p < 0.0001$), suggesting dysregulation of sphingolipid metabolism. Additionally, *ERCC2* and *MTA3* displayed 5′ hypermethylation (log2 fold changes 0.92, $p < 0.001$ and 0.74, $p < 0.01$), potentially impacting DNA repair and chromatin remodeling, respectively. *POLRMT* showed 3′ hypomethylation (log2 fold change −0.86, $p < 0.01$), which may affect mitochondrial gene expression. Furthermore, *AHNAK2* exhibited a mixed pattern of 5′ and 3′ hypermethylation (log2 fold changes 0.50, $p < 0.05$ and 0.82, $p < 0.01$), suggesting potential dysregulation of its structural and regulatory functions in various cellular processes. *ALDH3A2* displayed 3′ hypomethylation (log2 fold change −0.63, $p < 0.05$), which could impact its role in detoxifying aldehydes and maintaining cellular homeostasis. *CAPN5* showed significant 3′ hypermethylation (log2 fold change 0.82, $p < 0.01$), potentially affecting its proteolytic activity and regulatory functions in various cellular pathways. *TBP* exhibited a mixed pattern of 5′ and 3′ hypomethylation (log2 fold changes −0.49, $p < 0.05$ and −0.62, $p < 0.05$), suggesting potential dysregulation of its role as a general transcription factor. *TRMT61B* also showed 3′ hypomethylation (log2 fold change −0.57, $p < 0.05$), which could impact its function in tRNA modification and translation regulation. The observed DMR profiles across these genes have significant implications for understanding the pathophysiology of MIDD and its associated complications. Aberrant methylation patterns may influence various cellular processes, including retinal maintenance, immune surveillance, sphingolipid metabolism, DNA repair, chromatin remodeling, mitochondrial gene expression, structural and regulatory functions, detoxification, proteolysis, transcription, and translation regulation, ultimately impacting the manifestation and progression of MIDD and its related pathologies.

3.11. The integrated analysis of mtDNA variants and associated methylation patterns confirmed the probable crosstalk nucleus-mitochondria in MIDD

As done for gDNA, the integrated genomic and epigenetic analysis of mtDNA data provided insights into the relationship between specific gene variants and methylation levels across various mitochondrial loci. Several variants exhibited substantial differences in methylation levels between cases and controls. The m.8425A > C variant in the *MT-ATP8* gene, resulting in the missense mutation H34P, showed a marked increase in methylation levels in cases compared to controls. Likewise, the m.4769A > G variant in the *MT-ND2* gene, causing the I211L missense mutation, and the m.8063T > G variant in the *MT-CO2* gene, leading to the M140T missense mutation, both displayed higher methylation levels in cases. Conversely, some variants demonstrated lower methylation levels in cases relative to controls. The m.12425_12428del variant in the *MT-ND5* gene, causing a frameshift mutation, exhibited decreased methylation levels in cases. Additionally, the m.12662A > G (N109S) and m.13105A > G (I257V) variants in the *MT-ND5* gene, both resulting in missense mutations, also showed reduced methylation levels in cases. Interestingly, the m.8860A > G variant in the *MT-ATP6* gene, leading to the P123P synonymous mutation, showed higher methylation levels in cases, despite not altering the amino acid sequence. This suggests that epigenetic modifications may also influence gene regulation independent of protein-coding changes. Furthermore, the m.263A > G variant in the MT-D-loop region, a non-coding region involved in replication and transcription control, exhibited lower methylation levels in cases. This finding implies that variants in regulatory regions of the mitochondrial genome may also impact epigenetic patterns, potentially influencing gene expression and overall mitochondrial function. The observed differences in methylation levels associated with specific variants may be influenced by various factors, including variant heteroplasmy, as evidenced by the varying levels of heteroplasmy displayed in the inner tracks of Fig. 15, and the degree of conservation of the affected nucleotide positions across species, represented by the conservation scores. These findings suggest that specific mtDNA variants may influence or be associated with altered methylation patterns in the mitochondrial genome, potentially impacting the expression and regulation of mitochondrial genes. The differences in methylation levels between cases and controls could contribute to the phenotypic manifestations observed in the family by altering the expression and activity of essential mitochondrial proteins involved in processes such as oxidative phosphorylation, ATP synthesis, and mitochondrial dynamics.

4. Discussion

This study presents an in-depth analysis of the complex genetic and epigenetic landscape in a Sicilian family with MIDD. Through a comprehensive genomic approach, we have elucidated the intricate interplay between nuclear and mitochondrial DNA variations, epigenetic modifications, and their potential implications in the pathogenesis of MIDD. The main hypothesis is that mutations and methylation alterations in both mitochondrial and nuclear genes could impair related molecular mechanisms, ultimately leading to the MIDD phenotype observed in the family (Fig. 16).

4.1. Cross-talk between nuclear and mitochondrial genetics in MIDD pathogenesis

The WES analysis revealed a complex genetic landscape within the family, with a series of rare and deleterious variants in nuclear genes implicated in retinal homeostasis, mitochondrial function, and epigenetic regulation. The proband (II3) and the likely affected daughter (III1) carried a distinct set of shared variants in several genes, suggesting potential impairments in different cellular

Table 3

Genomic landscape of DMRs in gDNA of MIDD suspected family. The table shows DMRs identified in the proband compared to the healthy husband. The table presents the genomic coordinates, number of CpGs, beta coefficients, statistical significance, and genomic annotations for the top DMRs, highlighting genes associated with mitochondrial function, such as *EYS*, *ALMS1*, *SETBP1*, and *WDPCP*. Negative beta coefficients indicate hypomethylation, while positive values indicate hypermethylation. The table encompasses DMRs in various genomic regions, including promoters, exons, introns, and untranslated regions (UTRs).

GeneSymbol	start	end	width	CpGs	BetaCoefficient	statistic	p.value	q.value	direction	diff	CpGIsland	CpGShore	CpGShelf	OpenSea	annotation	DistanceToTSS
ALMS1	58017317	58118942	101626	2225	−0,1245	−13,1515	0,0000	0,0057	Hypermethylated	3	No	No	No	Yes	Promoter	0
	26723592	26881211	157620	3100	−0,0950	−11,3536	0,0000	0,0057	Hypermethylated	2	No	No	No	Yes	3′ UTR	193333
	105305125	105404847	99723	533	0,1246	7,8724	0,0002	0,0057	Hypermethylated	1	No	No	No	Yes	Promoter	0
EYS	93449478	93485986	36509	186	−0,7058	−63,9948	0,0000	0,0057	Hypermethylated	4	No	No	No	Yes	Exon	1343413
	228628174	228633746	5573	50	0,8788	15,8578	0,0000	0,0057	Hypomethylated	−3	No	No	No	Yes	Promoter	0
	43755465	43798903	43439	339	−0,3126	−10,4594	0,0000	0,0057	Hypomethylated	−2	No	No	No	Yes	Exon	1205841
	248256041	248344576	88536	534	0,2186	9,0538	0,0002	0,0057	Hypermethylated	4	No	No	No	Yes	Intron	1814585
	36134491	36243672	109182	2417	−0,0785	−8,8570	0,0002	0,0057	Hypomethylated	−3	No	No	No	Yes	Exon	752115
	63504870	63627056	122187	782	0,1211	8,8493	0,0002	0,0057	Hypermethylated	4	No	No	No	Yes	Intron	1530828
	35411070	35518755	107686	523	0,1922	8,8425	0,0002	0,0057	Hypermethylated	3	No	No	No	Yes	Intron	68671
	66555632	66706020	150389	919	0,1308	8,8287	0,0002	0,0057	Hypermethylated	3	No	No	No	Yes	Intron	1723115
	131423144	131476664	53521	630	0,2208	8,5358	0,0002	0,0057	Hypomethylated	−2	No	No	No	Yes	3′ UTR	332440
	89942723	89989458	46736	299	0,3085	7,8913	0,0002	0,0057	Hypomethylated	−3	No	No	No	Yes	Intron	231794
	189152290	189197089	44800	349	−0,1799	−7,7997	0,0002	0,0057	Hypermethylated	3	No	No	No	Yes	Exon	1046460
	167429350	167640988	211639	1169	0,0946	7,7583	0,0002	0,0057	Hypomethylated	−2	No	No	No	Yes	Intron	598890
	97805072	97977355	172284	870	−0,1089	−7,6605	0,0002	0,0057	Hypomethylated	−2	No	No	No	Yes	Exon	691900
LRRK2	42070459	42105079	34621	1596	−0,0595	−12,9126	0,0000	0,0057	Hypermethylated	3	No	No	No	Yes	3′ UTR	33115
LTBP1	85743328	85791769	48442	277	−0,3092	−8,5260	0,0002	0,0057	Hypermethylated	1	No	No	No	Yes	Promoter	0
MTA3	83446529	83571377	124849	688	−0,1635	−7,8412	0,0002	0,0057	Hypomethylated	−2	No	No	No	Yes	Promoter	0
	12529415	12536452	7038	57	−0,2255	−7,6429	0,0002	0,0057	Hypomethylated	−2	No	No	No	Yes	Promoter	0
MTBP	10401292	10453399	52108	364	0,2628	8,2677	0,0002	0,0057	Hypomethylated	−2	No	No	No	Yes	3′ UTR	18174
PTBP2	34571556	34793682	222127	5242	−0,0669	−14,8745	0,0000	0,0057	Hypermethylated	3	No	No	No	Yes	Distal Intergenic	−143055
	143518077	143539708	21632	99	−0,6356	−10,1395	0,0000	0,0057	Hypomethylated	−2	No	No	No	Yes	Exon	−34712
	109015432	109226860	211429	1231	0,1272	9,9668	0,0000	0,0057	Hypomethylated	−2	No	No	No	Yes	Promoter	0
SETBP1	21822332	21968399	146068	3519	−0,0835	−11,3960	0,0000	0,0057	Hypermethylated	5	No	No	No	Yes	Intron	159784
	61864466	61872523	8058	11	1,2699	8,6579	0,0002	0,0057	Hypomethylated	−3	Yes	Yes	Yes	Yes	Promoter	0
	171475208	171698746	223539	2002	0,0933	7,7632	0,0002	0,0057	Hypomethylated	−2	No	No	No	Yes	Exon	234023
TBPL2	42830081	43058267	228187	1364	−0,2094	−13,0568	0,0000	0,0057	Hypomethylated	−4	No	No	No	Yes	Distal Intergenic	−4718
USH2A	90574284	90697731	123448	706	0,1141	7,6060	0,0002	0,0057	Hypomethylated	−3	No	No	No	Yes	Exon	482167
	165042338	165087181	44844	263	−0,1847	−7,5565	0,0002	0,0057	Hypomethylated	−2	No	No	No	Yes	Exon	626440
WDPCP	62338117	62456624	118508	2316	−0,1224	−12,3556	0,0000	0,0057	Hypermethylated	3	No	No	No	Yes	Exon	80747
	189223014	189281213	58200	368	0,2669	11,0477	0,0000	0,0057	Hypomethylated	−4	No	No	No	Yes	Exon	141434
	77258925	77350773	91849	411	0,3003	9,0482	0,0002	0,0057	Hypomethylated	−2	No	No	No	Yes	3′ UTR	166362
	99416706	99484964	68259	366	−0,1357	−8,3937	0,0002	0,0057	Hypermethylated	2	No	No	No	Yes	Exon	4467
	123203238	123266560	63323	439	0,1223	7,5570	0,0002	0,0057	Hypomethylated	−1	No	No	No	Yes	Intron	280034

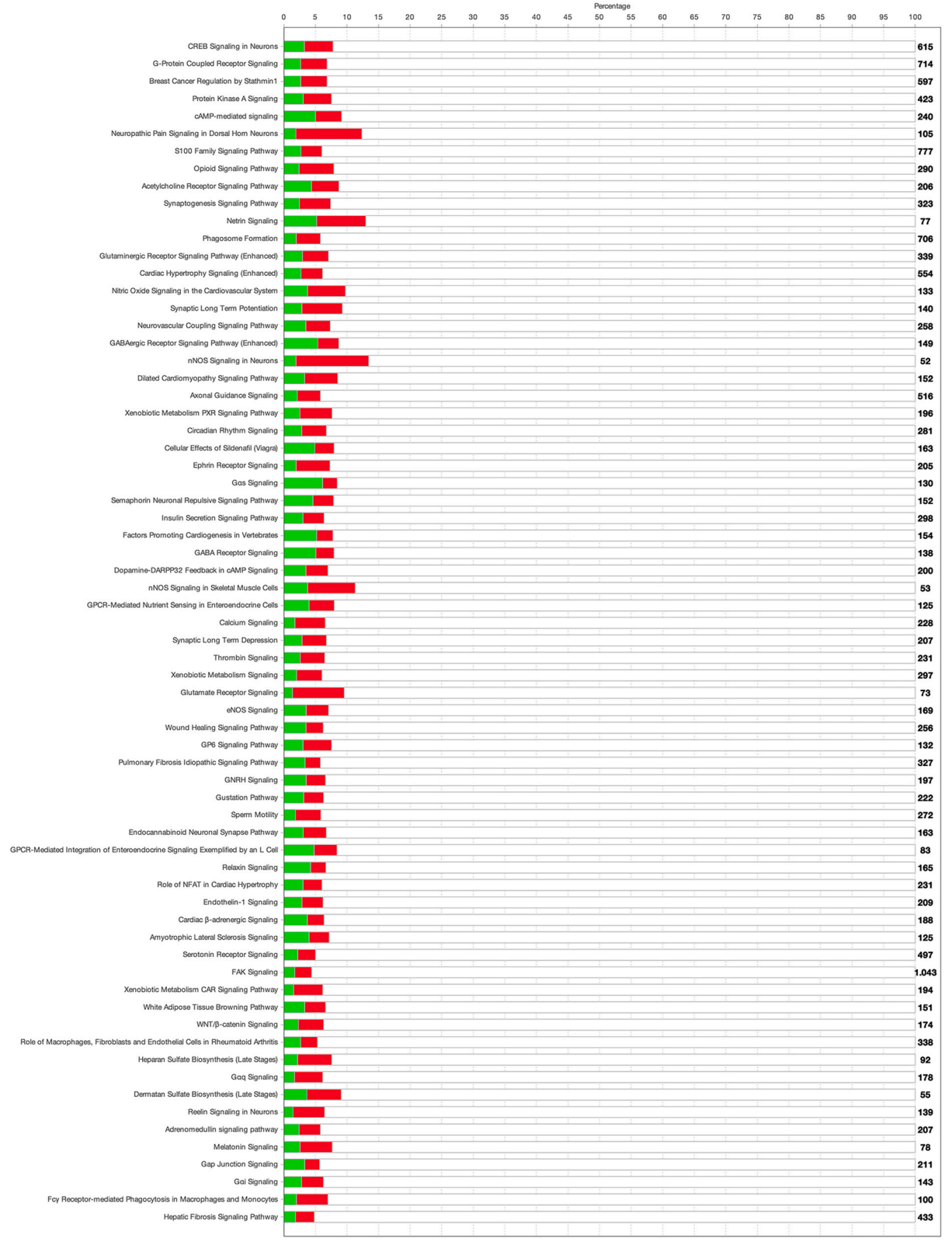

(caption on next page)

Fig. 10. Quantitative Assessment of Pathway Impact Using Vertical Stacked Bars. This chart visualizes the impact of various signaling pathways such as CREB, G-Protein Coupled Receptor, and Xenobiotic Metabolism, using stacked bars to indicate the level of pathway activity. Red bars highlight pathways where activity is decreased, while green bars signify pathways with increased activity. The magnitude of the effect is quantified using -log(p-value) along the x-axis, illustrating the statistical significance of the changes observed in these pathways.

processes, including retinal maintenance (*EYS*, *MKKS*, *RP1L1*, *USH2A*) [45–48], sphingolipid metabolism (*SPHK2*) [49], electron transport chain (*COQ4*) [50], structural and regulatory functions (*AHNAK2*) [51], and mitochondrial dynamics (*ALMS1*, *WDPCP*) [52,53]. Importantly, the presence of variants in genes like *COQ4* and *SPHK2*, which are involved in the electron transport chain and sphingolipid metabolism, respectively, highlights the direct link between nuclear genetics and mitochondrial function.

Among the mutated genes analyzed during pathway analysis, it emerged that *ERCC2* and *MTOR* are involved in the apoptotic process. Mitochondria play an essential role during apoptosis, particularly in the intrinsic pathway, also defined as the mitochondrial pathway. During the intrinsic pathway, cytochrome C enables the formation of the apoptosome [54]. Cell death of photoreceptors has an important role in retinal pathologies, including retinitis pigmentosa, leading to vision loss. In photoreceptors, mitochondrial apoptosis is mediated by the apoptosis inducing factor (AIF) located in the mitochondrial intermembrane space [55].

The *ERCC2* gene is implicated in the formation of the MMXD complex together with MIP18 and MMS19. This complex is essential for the formation of FeS clusters that takes place in the mitochondria. After being assembled in the mitochondria, they are transported to the cytoplasm. FeS clusters are necessary for the helicase activity carried out by XPD during transcription through binding with transcription factor IIH. The MMXD complex also has a role in mitotic spindle formation. The absence of the XPD protein determines an alteration in chromosomal segregation during mitosis. Moreover, the XPD protein plays a role in protecting nuclear and mitochondrial DNA from damage caused by ROS. Protection of nuclear DNA occurs when the protein is bound to transcription factor IIH. As for mitochondrial DNA, the protein is transported from the nucleus to the mitochondria when it is not bound to TFIIH [56]. A mutation in the *ERCC2* gene, therefore, could cause greater DNA damage in both the nucleus and mitochondria. In the nucleus, failure to repair UV damage can lead to pathologies such as xeroderma pigmentosum [57] and cerebro-oculo-facial-skeletal syndrome [58].

The *MTOR* gene is implicated in the formation of the mTORC1 and mTORC2 complexes. These two complexes have a phosphorylative activity. The molecules that undergo phosphorylation are fundamental in signal transduction, metabolic pathways and protein synthesis [59]. In the nucleus, mTORC1 is necessary for ribosome biosynthesis and transcription [60]. The mTORC1 complex also has a role in retinal blood vessel development [61]. At the mitochondrial level, mTORC1 is linked to mitochondrial biogenesis, oxidative metabolism and mitochondrial gene expression. In skeletal muscle in particular, it is associated with ATP production. mTORC2, instead, is mainly involved in oxidative metabolism [62].

The *MTOR* and *SPHK2* genes are involved in maintaining mitochondrial membrane structure [63]. The inner mitochondrial membrane is essential for oxidative phosphorylation and thus for energy production for the entire cell. The outer mitochondrial membrane is important for signal transduction, for example in the intrinsic apoptotic pathway [64]. A mutation in these two genes could alter the release of proteins directed to the nucleus and the entry of proteins coming from the nucleus.

The *TEFM* and *TRMT61B* genes are linked to mitochondrial gene expression. Mitochondrial DNA expression is a complex process involving maintenance of mitochondrial DNA, replication, transcription, processing of the primary transcript, RNA modifications, RNA stability, translation and insertion of translated proteins into the inner mitochondrial membrane. Not only proteins encoded by mitochondrial DNA itself, but also proteins encoded by nuclear DNA are used in these processes. Mitochondrial DNA encodes 13 proteins involved in oxidative phosphorylation [65]. An alteration of the proteins involved in mitochondrial gene expression could therefore lead to an alteration of oxidative phosphorylation and a lower amount of energy produced for the cell's metabolic processes.

The *TEFM* and *TRMT61B* genes are implicated in the metabolic processes of mitochondrial RNA. Most proteins required for mitochondrial RNA metabolism are encoded by nuclear genes. These proteins, therefore, must be transported inside the mitochondria to perform their function. Mutations that cause an alteration in mitochondrial RNA metabolism also have negative effects on mitochondrial DNA expression and cause pathologies related to oxidative phosphorylation. Various negative effects can stem from an alteration of oxidative phosphorylation including: an alteration of the cell's pH, an imbalance of metabolites due to an alteration of the inner membrane potential that causes problems in molecule transport, an increase in reactive oxygen species levels that damage DNA, and an alteration of the intrinsic apoptotic pathway [66].

The *TRMT61B* gene is associated, in particular, with the methylation of mitochondrial tRNA. tRNA methylation is fundamental for its structure and stability [67]. Mitochondrial tRNA, in particular, is methylated at positions 9 and 58 [68]. tRNA plays a role in protein synthesis and transport of amino acids to the membrane [69].

The *TEFM* and *STAT2* genes are involved in mitochondrial organization. Mutations in these genes could lead to alterations in oxidative phosphorylation.

The *TEFM* gene is implicated in combined oxidative phosphorylation deficiency 58. Oxidative phosphorylation is a process in which energy is produced for the entire cell. For this reason, an alteration at the level of this process causes problems in ATP production [70]. ATP is fundamental for cell growth and differentiation, thermogenesis and muscle movement [71]. Mutations in the *TEFM* gene could lead to alterations in the transcription of genes encoding proteins involved in oxidative phosphorylation complexes since TEFM has a role in mitochondrial transcription.

The *MKKS*, *RP1L1* and *USH2A* genes are linked to maintenance of photoreceptor cells. Photoreceptor cells are among the most vulnerable within the retina. Maintaining these cells is fundamental for visual function since they cannot be replaced once they have undergone degeneration [72]. Moreover, the presence of a high number of mitochondria is necessary within photoreceptors since

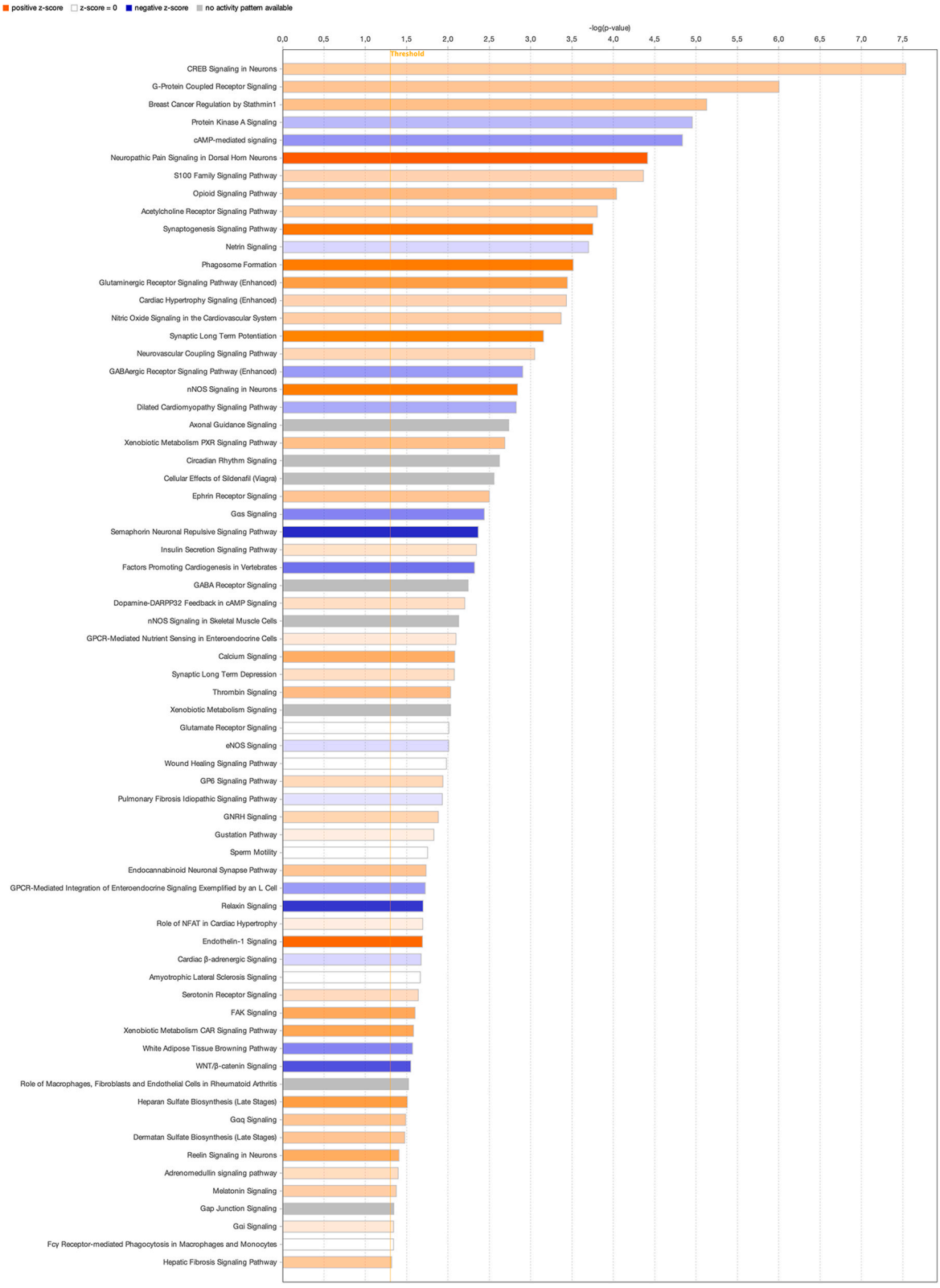

(caption on next page)

Fig. 11. Detailed Visualization of Pathway Activity Patterns in Horizontal Bars. This chart expands on the analysis of pathway significance by detailing the positive, negative, and inactive activity patterns across various biological pathways like Insulin Secretion, Cardiac Hypertrophy, and Hepatic Fibrosis. The orange bars indicate pathways with positive deviations from the norm, blue bars represent negative deviations, and gray bars indicate no significant activity pattern. The length of each bar is proportional to the -log(p-value), providing a clear metric of how significant the deviation is in each case. This detailed visualization helps in identifying the most critical pathways affected in the dataset.

phototransduction requires a large amount of energy [73]. Alterations in photoreceptor cell maintenance cause retinal dystrophies [72].

The *MKKS* and *WDPCP* genes are associated with primary cilium development. The primary cilium is a type of non-motile cilium with a role in signal transduction. At the retinal level, the outer segment of photoreceptors in particular is a modified cilium and has a role in phototransduction. It is also fundamental in rhodopsin transport. Mutations in these genes determine the development of syndromic or non-syndromic ciliopathies [73].

The *RP1L1* and *WDPCP* genes are involved in the axonemal structure. The latter is part of the cilia structure. For this reason, mutations in this gene cause ciliopathies [74].

The *MKKS*, *RP1L1* and *USH2A* genes are important in visual perception. Mutations in these genes cause vision loss in retinal dystrophies. In these pathologies, vision loss can be unilateral or bilateral and can be accompanied by loss of visual acuity and color vision [75].

The *RP1L1* and *USH2A* genes are associated with the photoreceptor connecting cilium. The connecting cilium is necessary for the connection between the outer and inner segments of photoreceptors. Alterations at the level of the connecting cilium determine dysfunctions in the transport of proteins (particularly those related to phototransduction) and ions between the two segments [76]. This also causes shortening of the outer segment. Moreover, energy utilization during transmission of the light signal and phagocytosis of the retinal pigment epithelium are affected [72].

The *WDPCP* gene is implicated in the cPLANE complex. The cPLANE complex has a role in ciliogenesis. For this reason, mutations in the genes involved in this complex lead to malformations and dysfunctions of cilia that can lead to the development of ciliopathies. The cPLANE complex also collaborates with the intraflagellar transport (IFT) system which is important in ciliogenesis and cilia-mediated signaling. The genes of the complex are also involved in planar cell polarity. It is also fundamental in the Hedgehog pathway which is linked to embryonic development, organogenesis and tissue homeostasis [77]. The *WDPCP* gene is, in fact, also involved in the development of sensory organs, particularly the eye, together with *RP1L1* and *USH2A*.

COQ4 and *SPHK2* variants exemplify the direct link between nuclear gene mutations and mitochondrial dysfunction. COQ4 is crucial for CoQ10 biosynthesis, an essential electron transport chain component, and its impairment can lead to reduced mitochondrial respiratory efficiency [78]. The SPHK2 gene is important for the biosynthetic process of sphingosine-1-phosphate. Sphingosine-1--phosphate plays a role at the mitochondrial level. Mutations in the SPHK2 gene can compromise ATP production in dopaminergic neurons. Moreover, sphingosine-1-phosphate is necessary for mitochondrial biogenesis and reduction of oxidative stress [63].

Alterations in these genes could thus compromise mitochondrial ATP production and increase oxidative stress, contributing to the cellular energy deficits observed in MIDD.

Complementing the nuclear genetic findings, the comprehensive analysis of mtDNA variants revealed a rich tapestry of genetic diversity across multiple mitochondrial genes and loci, including *MT-ND1*, *MT-ND2*, *MT-ND4*, *MT-ND5*, *MT-CO2*, *MT-CO3*, *MT-ATP6*, and *MT-ATP8*. These genes encode components of the electron transport chain and ATP synthesis machinery, essential for mitochondrial energy production [79].

The observed mtDNA variants, carried by both the proband (II3) and the daughter (III1), are likely to influence various mitochondrial processes, including oxidative phosphorylation, ATP synthesis, and mitochondrial dynamics. Variants in genes like *MT-ND1*, *MT-ND2*, *MT-ND4*, *MT-ND5*, *MT-CO2*, and *MT-CO3*, which encode subunits of the NADH dehydrogenase and cytochrome *c* oxidase complexes, could directly impact the efficiency of the electron transport chain and compromise ATP production. Variants in MT-ATP6 and *MT-ATP8*, which encode subunits of the ATP synthase complex, could further exacerbate the disruption of energy metabolism within the mitochondria.

The identification of variants in both nuclear and mitochondrial genes involved in similar cellular pathways, such as the electron transport chain and energy metabolism, provides strong evidence for the cross-talk between nuclear and mitochondrial genetics in MIDD pathogenesis. Dysfunctions in nuclear genes like *COQ4* and *SPHK2* could potentially contribute to mitochondrial dysfunction by impairing the electron transport chain and sphingolipid-mediated regulation of mitochondrial homeostasis. In turn, variants in mtDNA genes directly involved in the electron transport chain and ATP synthesis could further exacerbate the energy deficits and mitochondrial dysfunction, leading to a vicious cycle of cellular derangements.

4.2. Epigenetic modifications and their influence on nuclear and mitochondrial gene expression

The WGBS analysis uncovered a complex landscape of epigenetic modifications, with significant DMRs across the genome. The observed hypomethylation patterns, such as in the *EYS* gene, suggest pervasive epigenetic deregulation, potentially impacting genomic stability and gene expression regulation.

The complex interplay of methylation across genes like *ALMS1*, *WDPCP*, and *PTBP2* further demonstrates the nuanced influence of epigenetic modifications on gene regulation, with both hypermethylated and hypomethylated regions observed. These findings suggest that epigenetic modifications in nuclear genes can influence the expression of genes involved in mitochondrial function, further

Table 4

Comprehensive methylation landscape of mtDNA across selected regions. This table delineates the differential methylation profiles between case and control groups across various mitochondrial regions, showcasing the methylation levels, coverage, and Log_2 fold changes. "Region": the mitochondrial DNA segment under examination; "Cytosines": the number of cytosine nucleotides analyzed; "Case coverage" and "Control coverage": the sequencing depth in case and control samples, respectively; "Case coverage mean" and "Control coverage mean": the average sequencing depth per cytosine; "Case methylated" and "Control methylated": the count of methylated cytosines; "Case methylation level" and "Control methylation level": the proportion of methylated cytosines; "p-value": the statistical significance of methylation differences between case and control groups; "5′ gene" and "3′ gene": genes adjacent to the methylation site; "5′ distance" and "3′ distance": the proximity to these genes; "Log2_FC": the Log_2 fold change in methylation levels between cases and controls, indicating the magnitude of change. Notable regions such as 501.1000 and 10501.11000 are emphasized for their significant alterations in methylation patterns and their profound implications on gene expression and cellular energy metabolism.

Region	Cytosines	Case cover.	Case cover. mean	Case meth.	Case meth. level	Control coverage	Control coverage mean	Control meth.	Control meth. level	p-value	5′ gene	5′ dist.	3′ gene	3′ dist.	Log2 FC
1.500	28	2506	89,5000	101	0,0403	4192	149,7143	98	0,0234	6,809E-05			MT-TF	76	0,7858
1001..1500	32	3212	100,3750	148	0,0461	4180	130,6250	128	0,0306	3,418E-04	MT-RNR1	0	MT-TV	101	0,5895
2001..2500	12	1932	161,0000	61	0,0316	2912	242,6667	59	0,0203	9,002E-03	MT-RNR2	0	MT-TL1	729	0,6400
2501..3000	36	4437	123,2500	116	0,0261	5742	159,5000	116	0,0202	0,027471	MT-RNR2	0	MT-TL1	229	0,3720
3001..3500	42	6968	165,9048	209	0,0300	4941	117,6429	111	0,0225	6,852E-03	MT-RNR2	0	MT-TL1	0	0,4170
3501..4000	34	4729	139,0882	181	0,0383	7069	207,9118	203	0,0287	2,589E-03	MT-ND1	0	MT-TI	262	0,4145
5001..5500	22	9628	437,6364	240	0,0249	5475	248,8636	93	0,0170	7,078E-04	MT-ND2	0	MT-TW	11	0,5534
501..1000	30	2703	90,1000	137	0,0507	3376	112,5333	72	0,0213	3,474E-10			MT-TF	0	1,2489
5501..6000	26	2505	96,3462	103	0,0411	3569	137,2692	99	0,0277	2,796E-03	MT-ND2	0	MT-TW	0	0,5679
6001..6500	32	3141	98,1563	106	0,0337	4809	150,2813	130	0,0270	0,049443	MT-CO1	0	MT-TS1	945	0,3201
6501..7000	36	6798	188,8333	314	0,0462	4577	127,1389	153	0,0334	4,024E-04	MT-CO1	0	MT-TS1	445	0,4665
7001..7500	36	7927	220,1944	285	0,0360	4832	134,2222	109	0,0226	9,558E-06	MT-CO1	0	MT-TS1	0	0,6725
8001..8500	26	3351	128,8846	113	0,0337	5018	193,0000	128	0,0255	0,016894	MT-CO2	0	MT-TK	0	0,4027
9501..10000	28	9062	323,6429	188	0,0207	14872	531,1429	231	0,0155	1,825E-03	MT-CO3	0	MT-TG	0	0,4175
10501..11000	16	4488	280,5000	183	0,0408	7555	472,1875	161	0,0213	8,018E-10	MT-ND4L	0	MT-ND4	0	0,9361
11001..11500	26	5994	230,5385	157	0,0262	9200	353,8462	150	0,0163	1,824E-05	MT-ND4	0	MT-TH	637	0,6839
11501..12000	26	4775	183,6538	152	0,0318	7945	305,5769	166	0,0209	9,936E-05	MT-ND4	0	MT-TH	137	0,6074

(*continued on next page*)

Table 4 (*continued*)

Region	Cytosines	Case cover.	Case cover. mean	Case meth.	Case meth. level	Control coverage	Control coverage mean	Control meth.	Control meth. level	p-value	5′ gene	5′ dist.	3′ gene	3′ dist.	Log2 FC
12001..12500	14	3571	255,0714	110	0,0308	5738	409,8571	114	0,0199	5,955E-04	MT-ND4	0	MT-TH	0	0,6327
13501..14000	32	5019	156,8438	144	0,0287	10630	332,1875	236	0,0222	8,673E-03	MT-ND5	0	MT-ND6	148	0,3700
14001..14500	12	3683	306,9167	83	0,0225	6457	538,0833	82	0,0127	1,481E-04	MT-ND5	0	MT-ND6	0	0,8275
14501..15000	36	6872	190,8889	175	0,0255	10472	290,8889	171	0,0163	1,977E-05	MT-ND5	352	MT-ND6	0	0,6411
15001..15500	28	5747	205,2500	119	0,0207	9224	329,4286	140	0,0152	7,369E-03	MT-CYB	0	MT-TT	387	0,4481
16001..16500	20	2807	140,3500	104	0,0371	4044	202,2000	109	0,0270	0,011186	MT-TP	0			0,4590

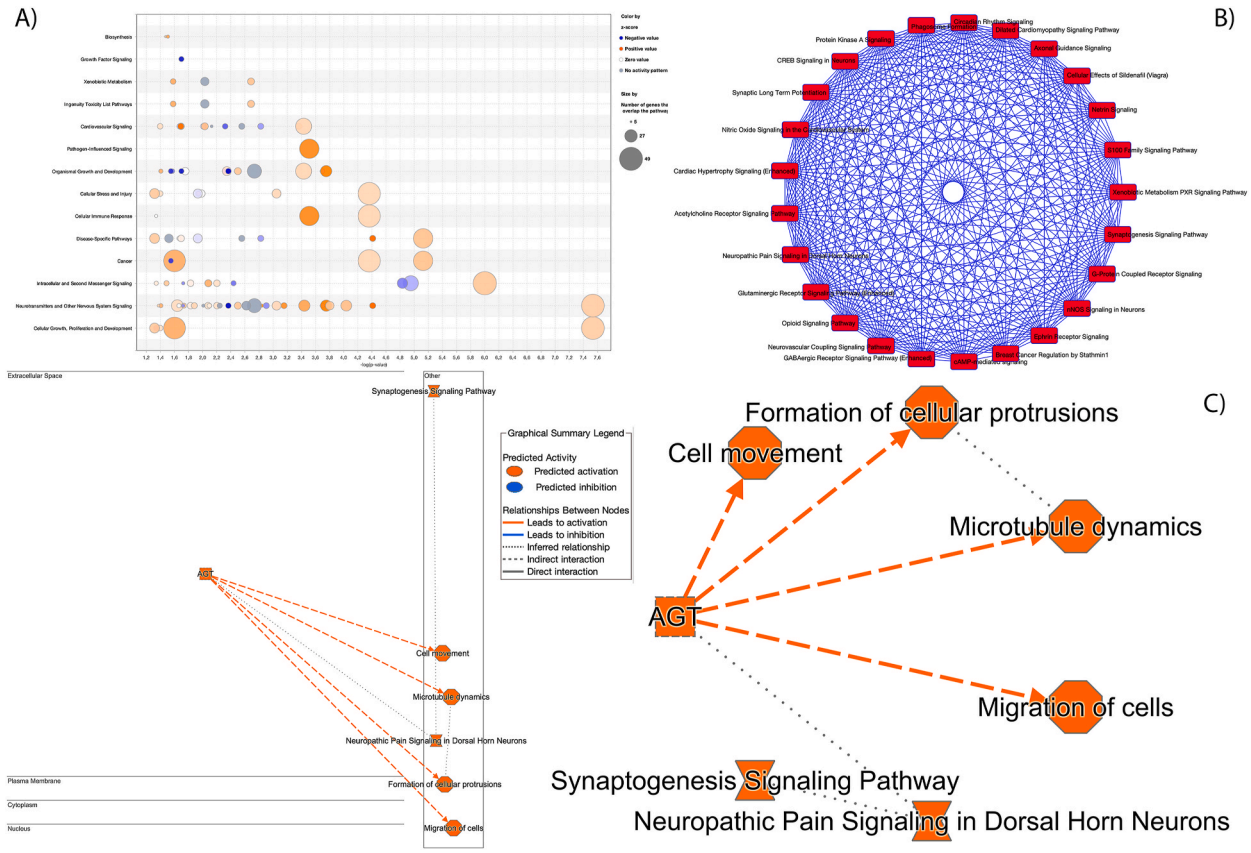

Fig. 12. Unveiling Key Disease Pathways and Biological Functions Through Advanced Molecular Analysis. Panel A presents a Canonical Pathways Bubble Chart, revealing central biosynthetic and signaling pathways. Panel B depicts Overlapping Canonical Pathways, indicating common molecular mechanisms. Panel C illustrates the predicted influence of AGT on cell dynamics and neuropathic pain, suggesting new therapeutic avenues.

reinforcing the cross-talk between nuclear and mitochondrial regulation. For instance, aberrant methylation patterns in *ALMS1*, which is implicated in microtubule organization and mitochondrial dynamics [80], could potentially disrupt the proper functioning of mitochondria and contribute to the cellular derangements observed in MIDD. Similarly, epigenetic modifications in *WDPCP*, which is involved in ciliogenesis and microtubule dynamics, could impact the distribution and trafficking of mitochondria within cells, further exacerbating mitochondrial dysfunction.

Furthermore, the analysis of mtDNA methylation patterns revealed significant variations across various mitochondrial regions, suggesting a nuanced landscape of epigenetic modulation within the mitochondrial genome. The observed differences in methylation levels between cases and controls, particularly in regions proximal to mitochondrial genes, underscore the intricate relationship between mtDNA methylation, gene expression, and mitochondrial functionality. Variations in methylation patterns near genes like MT-ND1, *MT-ND2*, *MT-ND4*, *MT-ND5*, *MT-CO2*, *MT-CO3*, *MT-ATP6*, and *MT-ATP8* could influence the expression and regulation of these crucial components of the electron transport chain and ATP synthesis machinery, further compromising mitochondrial bioenergetics [81].

The integration of WES and WGBS analyses revealed an extensive epigenetic variability across the whole genome, particularly across the gene loci and variants potentially associated with MIDD. Several genes exhibited variant-specific DMRs, demonstrating both hypermethylation and hypomethylation compared to the control sample.

The observed DMR profiles across genes involved in retinal degeneration (*LRRK2*) [82], immune surveillance (*KIR2DL1*, *KIR2DL3*) [83], sphingolipid metabolism (*SPHK2*), DNA repair (*ERCC2*), chromatin remodeling (*MTA3*) [84], mitochondrial gene expression (*POLRMT*) [85], structural and regulatory functions (*AHNAK2*), detoxification (*ALDH3A2*) [86], proteolysis (*CAPN5*) [87], transcription (*TBP*) [88], and translation regulation (*TRMT61B*) provide insights into the complex interplay between genetic variations and epigenetic modifications in MIDD pathogenesis. These epigenetic alterations could further contribute to the dysregulation of nuclear and mitochondrial gene expression, exacerbating the cellular derangements and mitochondrial dysfunction observed in MIDD.

4.3. Integrated Analysis of genetic and epigenetic profiles: insights into molecular mechanisms

The integrated analysis of mtDNA variants and associated methylation patterns revealed a potential crosstalk between nuclear and

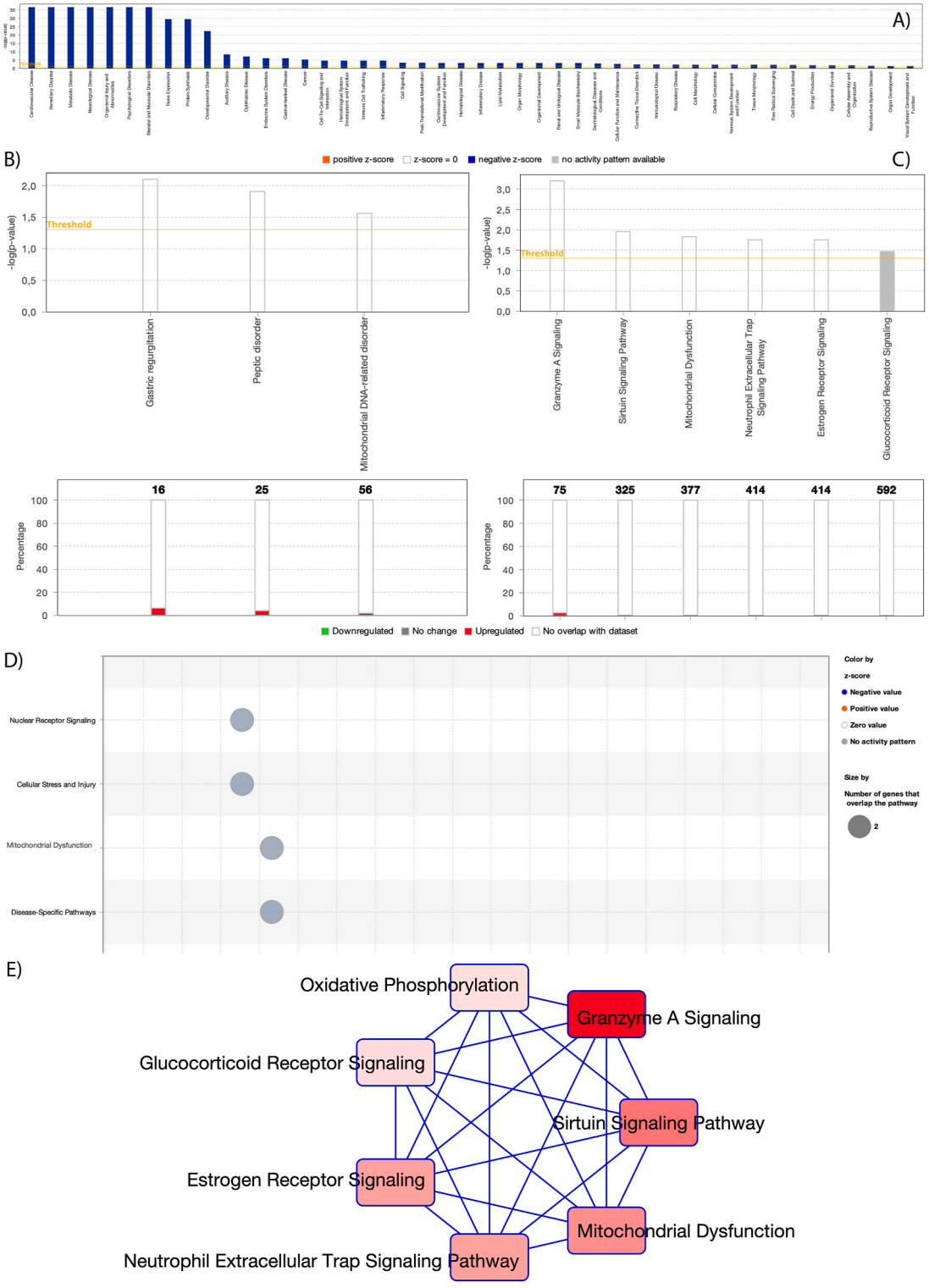

Fig. 13. Dissecting the Genetic and Epigenetic Landscape of mtDNA: a Comprehensive View of Mitochondrial Dysfunction and Its Potential Role in MIDD. This figure encapsulates the integrative findings from our latest research, providing a panoramic view of the molecular intricacies underlying a spectrum of hereditary and metabolic disorders. Panel A delineates Diseases and Bio-Functions, spotlighting critical areas such as Hereditary Disorder, Metabolic Disorder, and Ophthalmic Disease, underscoring the genetic and metabolic complexities driving these conditions. Panel B focuses on Machine Learning Disease Pathways, with an exclusive look at Mitochondrial DNA-related Disorder, highlighting the cutting-edge approach to uncovering the genetic roots of mitochondrial dysfunctions. Panel C and D, both dedicated to Canonical Pathways, converge on

Mitochondrial Dysfunction, emphasizing its pivotal role across various disease states and its impact on cellular metabolism and energy production. Panel E, Overlapping Canonical Pathways, reinforces the centrality of Mitochondrial Dysfunction, illustrating its ubiquitous influence across the analyzed conditions and suggesting a universal target for therapeutic intervention. Together, these panels offer a comprehensive snapshot of the current state of knowledge on the molecular mechanisms of disease, pointing to mitochondrial health as a key factor in the pathogenesis of MIDD.

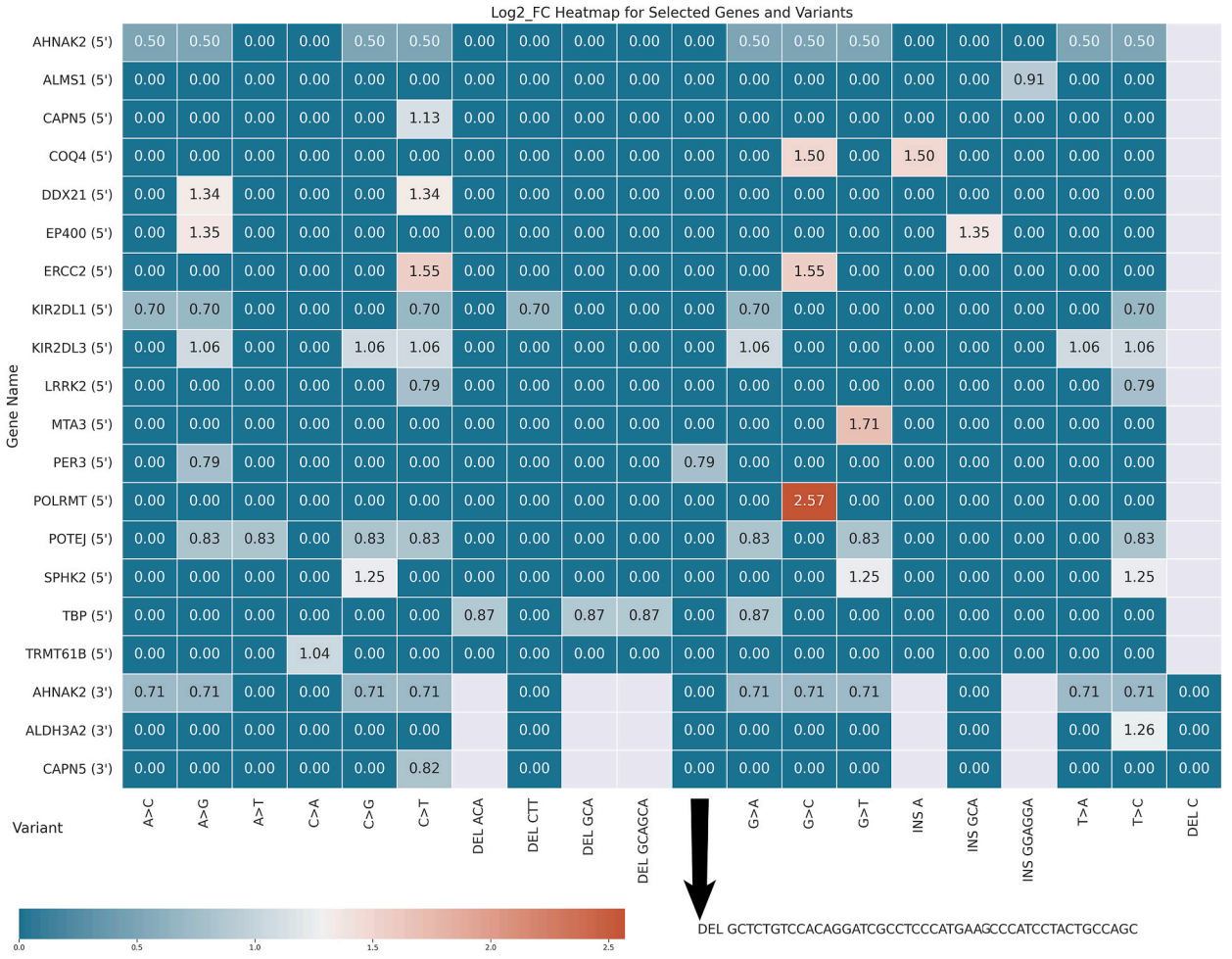

Fig. 14. Differential Methylation Landscape across Epigenetic and Mitochondrial Homeostasis-related Nuclear Genes. The figure showcases a heatmap that elucidates the differential methylation patterns of nuclear genes associated with epigenetic regulation and mitochondrial function. The Log2 Fold Change (FC) values, calculated by comparing individual II3 against II4, illuminate the methylation dynamics at CpG-rich regions of the genes, either at the 5′ or 3′ ends.
The intensity of the colors in the heatmap reflects the degree of change in methylation levels between the two individuals. Genes with increased methylation at the 5′ end might indicate regulatory regions where hypermethylation could lead to gene silencing. Conversely, genes with decreased methylation at the 3′ end could suggest regions where hypomethylation might enhance gene expression.

mitochondrial regulation in MIDD. Several variants exhibited substantial differences in methylation levels between cases and controls, including variants in the *MT-ATP8*, *MT-ND2*, MT-CO2, *MT-ND5*, and *MT-ATP6* genes, as well as the non-coding MT-D-loop region.

These findings suggest that specific mtDNA variants may influence or be associated with altered methylation patterns in the mitochondrial genome, potentially impacting the expression and regulation of mitochondrial genes. For instance, the m.8425A > C variant in *MT-ATP8*, which leads to the H34P missense mutation, exhibited increased methylation levels in cases compared to controls. This variant, combined with the altered methylation patterns, could further compromise the function of the ATP synthase complex and exacerbate the energy deficits within the mitochondria [89].

Similarly, variants in the *MT-ND2* (m.4769A > G, I211L), *MT-CO2* (m.8063T > G, M140T), and *MT-ND5* (m.12425_12428del, frameshift) genes, which are involved in the electron transport chain, also showed differences in methylation levels between cases and controls. These findings suggest that the interplay between genetic variations and epigenetic modifications could have a synergistic effect on mitochondrial dysfunction, further disrupting the electron transport chain and ATP synthesis [90,91].

Interestingly, even the m.8860A > G variant in *MT-ATP6*, which results in a synonymous mutation (P123P), exhibited increased

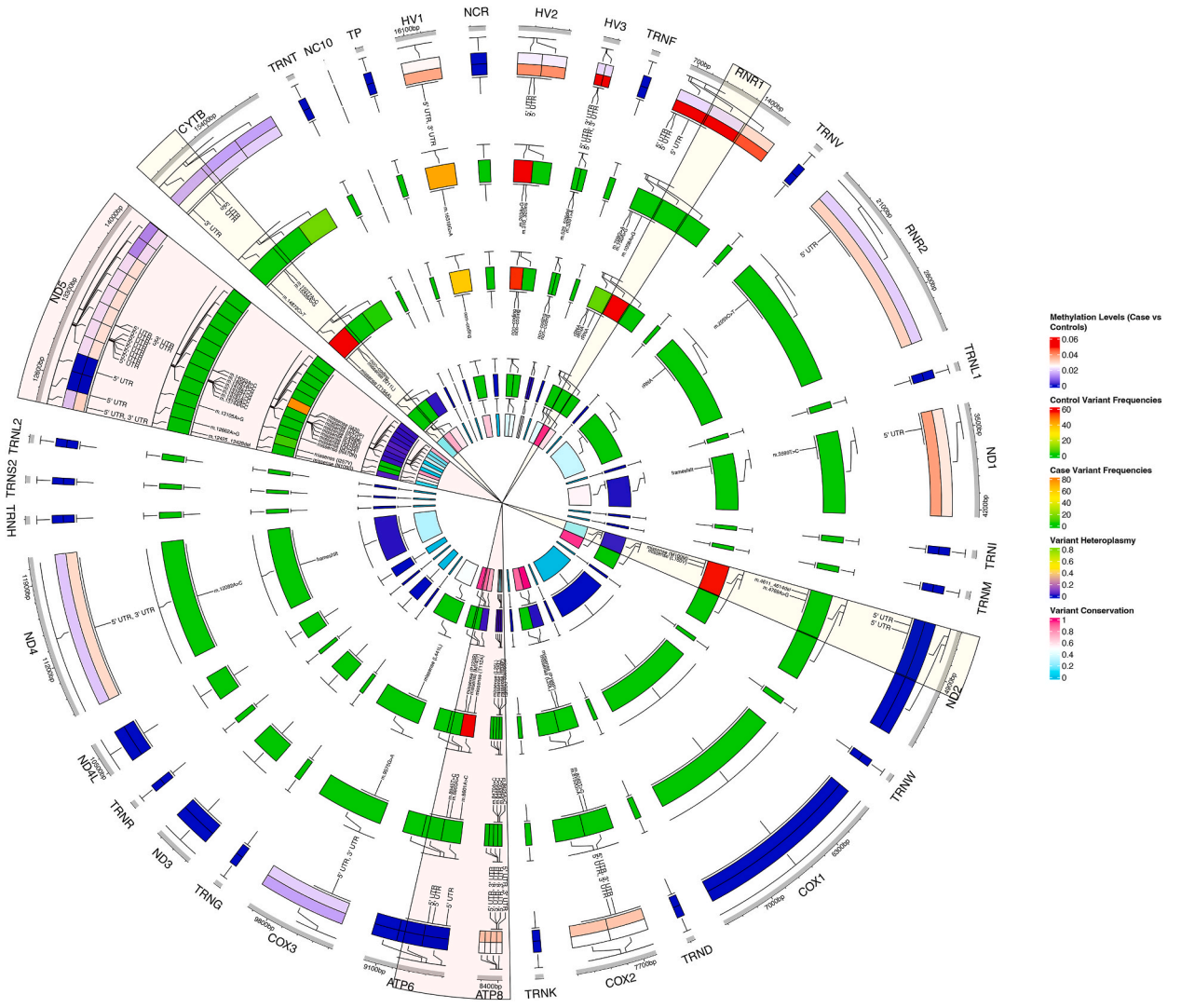

Fig. 15. Circular Visualization of the Human Mitochondrial Genome and Associated Variant Information. The circular plot depicts the human mitochondrial genome, with various features such as protein-coding genes (e.g., *MT-ND1*, *MT-CO1*), tRNAs, and non-coding regions (e.g., D-loop) annotated along the perimeter. The inner tracks display variant-specific information, including methylation levels in cases and controls, variant frequencies, variant heteroplasmy, and conservation scores across species. Several variants, highlighted in the figure, exhibit notable differences in methylation levels between cases and controls, suggesting potential associations between specific mtDNA variants and altered epigenetic patterns. The observed differences in methylation may influence the expression and regulation of mitochondrial genes, contributing to the phenotypic manifestations observed in the study population.

methylation levels in cases. This observation highlights the potential influence of epigenetic modifications on gene regulation, independent of protein-coding changes, further emphasizing the complex interplay between genetic and epigenetic factors [92].

The observed differences in methylation levels between cases and controls could contribute to the phenotypic manifestations observed in the family by altering the expression and activity of essential mitochondrial proteins involved in processes such as oxidative phosphorylation, ATP synthesis, and mitochondrial dynamics.

The pathway analyses of mtDNA mutated genes carried by the family members delineated a complex interplay among genetic predispositions, metabolic dysfunctions, and cellular derangements underpinning a spectrum of symptoms, including hereditary, metabolic, neurological, ophthalmic, and endocrine disorders, alongside pronounced inflammatory responses. Notably, the emphasis on mitochondrial bioenergetics, with oxidative phosphorylation and mitochondrial dysfunction emerging as critical nodes within the pathophysiological landscape, underscores the organelle's pivotal role in cellular energetics and survival.

The identification of mitochondrial DNA-related disorder through machine learning disease pathway analysis corroborates the significant impact of mitochondrial genetics on systemic health. The recurrence of mitochondrial dysfunction across various analysis panels underscores its central role in disease mechanisms, impacting processes ranging from lipid metabolism and small molecule biochemistry to energy production and cellular assembly.

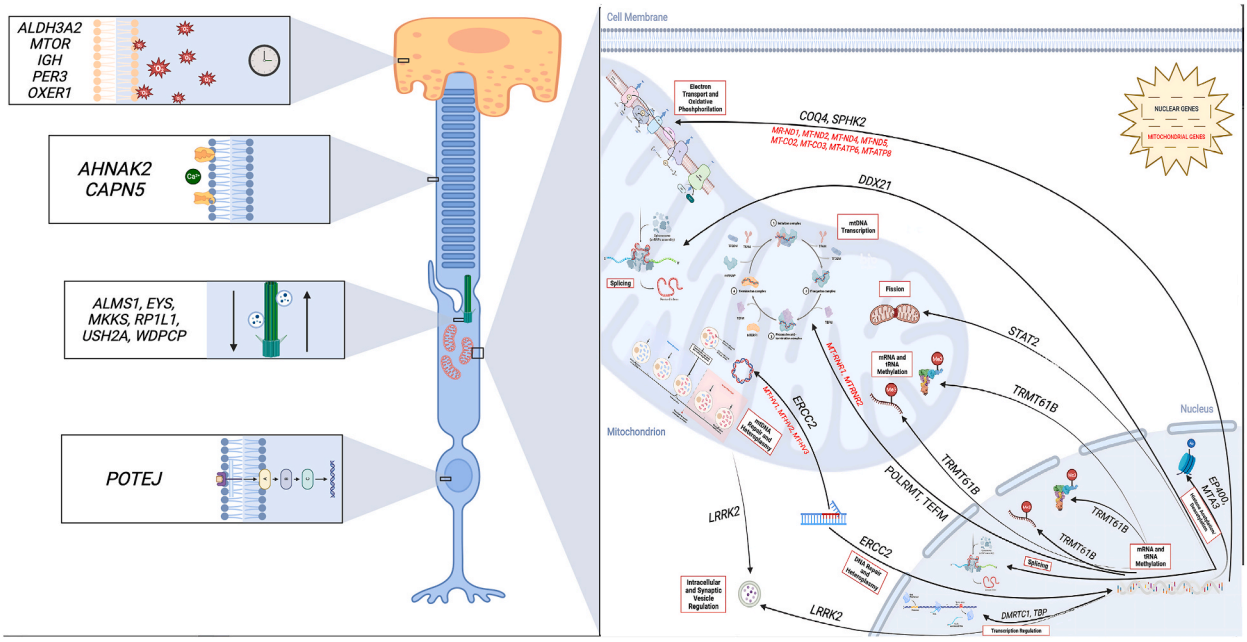

Fig. 16. Nuclear-mitochondrial cross-talk hypothesis in MIDD pathogenesis. The figure summarizes the central hypothesis of the research article, which proposes that mutations and methylation alterations in both nuclear and mitochondrial genes could impair related molecular mechanisms, ultimately leading to the MIDD phenotype observed in the family under study. The nucleus, represented by the blue oval, contains the nuclear DNA (nDNA), which is depicted as a double helix. Several genes of interest, including *ALDH3A2*, *ALMS1*, *CAPN5*, *COQ4*, *EYS*, *MKKS*, *MTOR*, *POTEJ*, *RP1L1*, *SPHK2*, *USH2A*, and *WDPCP*, are labeled in the nucleus. These genes are implicated in various cellular processes, such as retinal homeostasis, mitochondrial function, and epigenetic regulation. The mitochondrion, illustrated as a green structure, contains the mtDNA, shown as a circular molecule. Several mitochondrial genes, including *MT-ND1*, *MT-ND2*, *MT-ND4*, *MT-ND5*, *MT-CO2*, *MT-CO3*, *MT-ATP6*, and *MT-ATP8*, are labeled within the mitochondrion. These genes encode components of the electron transport chain and ATP synthesis machinery, essential for mitochondrial energy production. The figure emphasizes the cross-talk between the nucleus and the mitochondria through several interconnecting arrows. These arrows represent the potential influence of nuclear gene variants and epigenetic modifications on mitochondrial function, as well as the impact of mtDNA variants and epigenetic changes on nuclear gene expression and regulation. The cross-talk between the nucleus and mitochondria, mediated by genetic and epigenetic factors, plays a crucial role in the pathogenesis of MIDD, as evidenced by the complex interplay of nuclear and mitochondrial gene variants, epigenetic modifications, and their potential impact on cellular processes and mitochondrial function.

Furthermore, the analysis highlights the significance of free radical scavenging in combating oxidative stress, a key contributor to mitochondrial and cellular damage, especially pertinent in the retinal dysfunction associated with MIDD. The inclusion of visual system development and function, alongside nervous system development, emphasizes the critical impact of mitochondrial function on sensory and neurological health, indicating that aberrations in mtDNA methylation could directly influence the phenotypic manifestations of MIDD, including its retinal aspects.

The observed dysregulation in pathways related to cellular stress and injury, and neuropathic pain signaling in dorsal horn neurons, further suggests that the impact of mitochondrial dysfunction extends beyond energy production, affecting various cellular processes and contributing to the broader spectrum of disease pathology.

5. Conclusions

In conclusion, this study has unveiled a complex interplay between nuclear and mitochondrial genetics, epigenetic modifications, and their potential impact on the pathogenesis of MIDD. The identification of rare and deleterious variants across multiple nuclear and mitochondrial genes, the elucidation of mtDNA variations with varying heteroplasmy levels, and the comprehensive analysis of epigenetic profiles, including both nuclear and mitochondrial methylation patterns, have provided valuable insights into the molecular mechanisms underlying this complex disorder. The integration of these data has highlighted the potential crosstalk between nuclear and mitochondrial regulation, with specific mtDNA variants influencing methylation patterns and potentially impacting the expression and regulation of mitochondrial genes. The observed dysregulation in pathways related to mitochondrial dysfunction, cellular stress, and injury, as well as neuropathic pain signaling, underscores the broad spectrum of cellular processes affected by mitochondrial health.

To further validate these findings and deepen our understanding of the molecular intricacies of MIDD, it will be fundamental to widen the patients' cohort, and functionally evaluate obtained findings by a suite of mitochondrial assays. These assays, encompassing mitochondrial respiration assessments (e.g., oxygen consumption rate, ATP production rates), reactive oxygen species measurement, mitochondrial membrane potential assessment, mitochondrial mass and morphology examination, citrate synthase activity, epigenetic

modifications analysis confirmation (e.g., TFAM modification studies), proteomic and metabolomic profiling, and reporter gene assays, are crucial. Such comprehensive functional validations will elucidate the direct impacts of genetic and epigenetic alterations on mitochondrial function, further clarifying the nuclear-mitochondrial crosstalk mechanisms. Implementing these methodologies will bolster the evidence for the proposed mechanisms of MIDD pathogenesis and aid in the identification of novel biomarkers and therapeutic targets. These future directions are essential for advancing toward targeted therapeutic interventions and personalized approaches to disease management, offering hope for improved outcomes in MIDD and related mitochondrial dysfunctions.

5.1. Ethics statement

This study was approved by the ethics committee of the "Azienda Policlinico Universitario di Messina" (approval number: 23/17bis, prot. n. 0014661). All procedures involving human participants were performed in accordance with institutional and/or national research committee ethical standards and performed in accordance with the 1964 Declaration of Helsinki and its later amendments or comparable ethical standards. The participants gave written informed consent for the publication of any images, clinical data and other data included in the manuscript.

Funding

This research received no external funding.

Data availability

The data are available as supplementary materials and upon request.

CRediT authorship contribution statement

Luigi Donato: Writing – original draft, Methodology, Formal analysis, Data curation, Conceptualization. **Concetta Scimone:** Formal analysis, Data curation. **Simona Alibrandi:** Formal analysis, Data curation, Conceptualization. **Maria Vadalà:** Methodology, Investigation, Formal analysis. **Massimo Castellucci:** Methodology, Investigation, Formal analysis. **Vincenza Maria Elena Bonfiglio:** Methodology, Investigation, Formal analysis. **Sergio Zaccaria Scalinci:** Methodology, Formal analysis, Data curation. **Giorgia Abate:** Methodology, Investigation, Data curation. **Rosalia D'Angelo:** Writing – review & editing, Visualization, Supervision, Data curation. **Antonina Sidoti:** Writing – review & editing, Validation, Supervision.

Declaration of competing interest

The authors declare that they have no known competing financial interests or personal relationships that could have appeared to influence the work reported in this paper.

Appendix A. Supplementary data

Supplementary data to this article can be found online at https://doi.org/10.1016/j.heliyon.2024.e34756.

References

[1] S.H. Tsang, A.R.P. Aycinena, T. Sharma, Mitochondrial disorder: maternally inherited diabetes and deafness, Adv. Exp. Med. Biol. 1085 (2018) 163–165.
[2] H.Z. Li, R.Y. Li, M. Li, A review of maternally inherited diabetes and deafness, Front Biosci (Landmark Ed) 19 (5) (2014) 777–782.
[3] R. Murphy, et al., Clinical features, diagnosis and management of maternally inherited diabetes and deafness (MIDD) associated with the 3243A>G mitochondrial point mutation, Diabet. Med. 25 (4) (2008) 383–399.
[4] P.L. Muller, et al., Progression of retinopathy secondary to maternally inherited diabetes and deafness - evaluation of predicting parameters, Am. J. Ophthalmol. 213 (2020) 134–144.
[5] N. Oishi, et al., Multimodal imaging analysis of macular dystrophy in patient with maternally inherited diabetes and deafness (MIDD) with m.3243A>G mutation, Ophthalmic Genet. 42 (3) (2021) 304–311.
[6] J. Birtel, et al., Mitochondrial retinopathy, Ophthalmol Retina 6 (1) (2022) 65–79.
[7] S.J. Annesley, P.R. Fisher, Mitochondria in health and disease, Cells 8 (7) (2019).
[8] A.H. Ludwig-Slomczynska, M. Rehm, Mitochondrial genome variations, mitochondrial-nuclear compatibility, and their association with metabolic diseases, Obesity 30 (6) (2022) 1156–1169.
[9] L. Donato, et al., Possible A2E mutagenic effects on RPE mitochondrial DNA from innovative RNA-seq bioinformatics pipeline, Antioxidants 9 (11) (2020).
[10] A. Hahn, S. Zuryn, The cellular mitochondrial genome landscape in disease, Trends Cell Biol. 29 (3) (2019) 227–240.
[11] J.M. van den Ouweland, et al., Maternally inherited diabetes and deafness (MIDD): a distinct subtype of diabetes associated with a mitochondrial tRNA(Leu) (UUR) gene point mutation, Muscle Nerve 3 (1995) S124–S130. Suppl.
[12] M.R. Chiaratti, et al., Oocyte mitochondria: role on fertility and disease transmission, Anim. Reprod. 15 (3) (2018) 231–238.
[13] M. Vallet-Buisan, et al., Contribution of semen to early embryo development: fertilization and beyond, Hum. Reprod. Update 29 (4) (2023) 395–433.
[14] G.B. Stefano, et al., Mitochondrial heteroplasmy, Adv. Exp. Med. Biol. 982 (2017) 577–594.

[15] K.N. Robinson, et al., The role of heteroplasmy in the diagnosis and management of maternally inherited diabetes and deafness, Endocr. Pract. 26 (2) (2020) 241–246.
[16] M. Yang, et al., The mutations and clinical variability in maternally inherited diabetes and deafness: an analysis of 161 patients, Front. Endocrinol. 12 (2021) 728043.
[17] B. Disha, et al., Mitochondria in biology and medicine - 2023, Mitochondrion (2024) 101853.
[18] C. Saint-Martin, et al., Gene panel sequencing of patients with monogenic diabetes brings to light genes typically associated with syndromic presentations, Diabetes 71 (3) (2022) 578–584.
[19] S. Henikoff, J.M. Greally, Epigenetics, cellular memory and gene regulation, Curr. Biol. 26 (14) (2016) R644–R648.
[20] J.C. Alcolado, K. Laji, R. Gill-Randall, Maternal transmission of diabetes, Diabet. Med. 19 (2) (2002) 89–98.
[21] L. Zhang, Q. Lu, C. Chang, Epigenetics in health and disease, Adv. Exp. Med. Biol. 1253 (2020) 3–55.
[22] L. Donato, et al., Human retinal secretome: a cross-link between mesenchymal and retinal cells, World J Stem Cells 15 (7) (2023) 665–686.
[23] K. Wang, M. Li, H. Hakonarson, ANNOVAR: functional annotation of genetic variants from high-throughput sequencing data, Nucleic Acids Res. 38 (16) (2010) e164.
[24] T. Koressaar, et al., Primer3_masker: integrating masking of template sequence with primer design software, Bioinformatics 34 (11) (2018) 1937–1938.
[25] L.N. Singh, et al., MitoScape: a big-data, machine-learning platform for obtaining mitochondrial DNA from next-generation sequencing data, PLoS Comput. Biol. 17 (11) (2021) e1009594.
[26] S.L. Battle, et al., A bioinformatics pipeline for estimating mitochondrial DNA copy number and heteroplasmy levels from whole genome sequencing data, NAR Genom Bioinform 4 (2) (2022) lqac034.
[27] M.T. Lott, et al., mtDNA variation and analysis using Mitomap and mitomaster, Curr Protoc Bioinformatics 44 (123) (2013) 1–26, 1 23.
[28] L. Shen, M.J. Falk, X. Gai, MSeqDR quick-mitome (QM): combining phenotype-guided variant interpretation and machine learning classifiers to aid primary mitochondrial disease genetic diagnosis, Curr Protoc 4 (1) (2024) e955.
[29] M. Bernt, et al., MITOS: improved de novo metazoan mitochondrial genome annotation, Mol. Phylogenet. Evol. 69 (2) (2013) 313–319.
[30] C. Calabrese, et al., MToolBox: a highly automated pipeline for heteroplasmy annotation and prioritization analysis of human mitochondrial variants in high-throughput sequencing, Bioinformatics 30 (21) (2014) 3115–3117.
[31] J. Damas, et al., MitoBreak: the mitochondrial DNA breakpoints database, Nucleic Acids Res. 42 (Database issue) (2014) D1261–D1268.
[32] S. Castellana, et al., MitImpact 3: modeling the residue interaction network of the Respiratory Chain subunits, Nucleic Acids Res. 49 (D1) (2021) D1282–D1288.
[33] R. Preste, et al., HmtVar: a new resource for human mitochondrial variations and pathogenicity data, Nucleic Acids Res. 47 (D1) (2019) D1202–D1210.
[34] L.C. Wong, et al., Interpretation of mitochondrial tRNA variants, Genet. Med. 22 (5) (2020) 917–926.
[35] L. Li, et al., Msuite2: all-in-one DNA methylation data analysis toolkit with enhanced usability and performance, Comput. Struct. Biotechnol. J. 20 (2022) 1271–1276.
[36] K.D. Hansen, B. Langmead, R.A. Irizarry, BSmooth: from whole genome bisulfite sequencing reads to differentially methylated regions, Genome Biol. 13 (10) (2012) R83.
[37] Y. Park, et al., MethylSig: a whole genome DNA methylation analysis pipeline, Bioinformatics 30 (17) (2014) 2414–2422.
[38] F. Juhling, et al., metilene: fast and sensitive calling of differentially methylated regions from bisulfite sequencing data, Genome Res. 26 (2) (2016) 256–262.
[39] A. Akalin, et al., methylKit: a comprehensive R package for the analysis of genome-wide DNA methylation profiles, Genome Biol. 13 (10) (2012) R87.
[40] D.E. Condon, et al., Defiant: (DMRs: easy, fast, identification and ANnoTation) identifies differentially Methylated regions from iron-deficient rat hippocampus, BMC Bioinf. 19 (1) (2018) 31.
[41] B.I. Laufer, et al., Low-pass whole genome bisulfite sequencing of neonatal dried blood spots identifies a role for RUNX1 in Down syndrome DNA methylation profiles, Hum. Mol. Genet. 29 (21) (2021) 3465–3476.
[42] G. Bindea, et al., ClueGO: a Cytoscape plug-in to decipher functionally grouped gene ontology and pathway annotation networks, Bioinformatics 25 (8) (2009) 1091–1093.
[43] G. Bindea, J. Galon, B. Mlecnik, CluePedia Cytoscape plugin: pathway insights using integrated experimental and in silico data, Bioinformatics 29 (5) (2013) 661–663.
[44] P. Shannon, et al., Cytoscape: a software environment for integrated models of biomolecular interaction networks, Genome Res. 13 (11) (2003) 2498–2504.
[45] C. Wei, et al., Novel compound heterozygous EYS variants may be associated with arRP in a large Chinese pedigree, Biosci. Rep. 40 (6) (2020).
[46] R.A. Rachel, et al., Combining Cep290 and Mkks ciliopathy alleles in mice rescues sensory defects and restores ciliogenesis, J. Clin. Invest. 122 (4) (2012) 1233–1245.
[47] N.C.L. Noel, I.M. MacDonald, RP1L1 and inherited photoreceptor disease: a review, Surv. Ophthalmol. 65 (6) (2020) 725–739.
[48] L. Toualbi, M. Toms, M. Moosajee, USH2A-retinopathy: from genetics to therapeutics, Exp. Eye Res. 201 (2020) 108330.
[49] H. Porter, et al., Characterizing sphingosine kinases and sphingosine 1-phosphate receptors in the mammalian eye and retina, Int. J. Mol. Sci. 19 (12) (2018).
[50] L. Pelosi, et al., COQ4 is required for the oxidative decarboxylation of the C1 carbon of coenzyme Q in eukaryotic cells, Mol Cell 84 (5) (2024).
[51] M. Zardab, et al., The obscure potential of AHNAK2, Cancers 14 (3) (2022).
[52] M. Alvarez-Satta, et al., ALMS1 regulates TGF-beta signaling and morphology of primary cilia, Front. Cell Dev. Biol. 9 (2021) 623829.
[53] M.T. Langhans, et al., Wdpcp regulates cellular proliferation and differentiation in the developing limb via hedgehog signaling, BMC Dev. Biol. 21 (1) (2021) 10.
[54] F.J. Bock, S.W.G. Tait, Mitochondria as multifaceted regulators of cell death, Nat. Rev. Mol. Cell Biol. 21 (2) (2020) 85–100.
[55] W. Liu, et al., Retinitis pigmentosa: progress in molecular pathology and biotherapeutical strategies, Int. J. Mol. Sci. 23 (9) (2022).
[56] B.V. Houten, J. Kuper, C. Kisker, Role of XPD in cellular functions: to TFIIH and beyond, DNA Repair 44 (2016) 136–142.
[57] A.K. Leung, et al., Xeroderma pigmentosum: an updated review, Drugs Context 11 (2022).
[58] H. Suzumura, O. Arisaka, Cerebro-oculo-facio-skeletal syndrome, Adv. Exp. Med. Biol. 685 (2010) 210–214.
[59] A. Szwed, E. Kim, E. Jacinto, Regulation and metabolic functions of mTORC1 and mTORC2, Physiol. Rev. 101 (3) (2021) 1371–1426.
[60] M. Jhanwar-Uniyal, et al., Diverse signaling mechanisms of mTOR complexes: mTORC1 and mTORC2 in forming a formidable relationship, Adv Biol Regul 72 (2019) 51–62.
[61] T. Nakahara, et al., Mammalian target of Rapamycin (mTOR) as a potential therapeutic target in pathological ocular angiogenesis, Biol. Pharm. Bull. 40 (12) (2017) 2045–2049.
[62] M. Linke, et al., mTORC1 and mTORC2 as regulators of cell metabolism in immunity, FEBS Lett. 591 (19) (2017) 3089–3103.
[63] K. Hodun, A. Chabowski, M. Baranowski, Sphingosine-1-phosphate in acute exercise and training, Scand. J. Med. Sci. Sports 31 (5) (2021) 945–955.
[64] M. Giacomello, et al., The cell biology of mitochondrial membrane dynamics, Nat. Rev. Mol. Cell Biol. 21 (4) (2020) 204–224.
[65] C.M. Gustafsson, M. Falkenberg, N.G. Larsson, Maintenance and expression of mammalian mitochondrial DNA, Annu. Rev. Biochem. 85 (2016) 133–160.
[66] T.J. Nicholls, J. Rorbach, M. Minczuk, Mitochondria: mitochondrial RNA metabolism and human disease, Int. J. Biochem. Cell Biol. 45 (4) (2013) 845–849.
[67] C. Zhang, G. Jia, Reversible RNA modification N(1)-methyladenosine (m(1)A) in mRNA and tRNA, Dev. Reprod. Biol. 16 (3) (2018) 155–161.
[68] J. Li, H. Zhang, H. Wang, N(1)-methyladenosine modification in cancer biology: current status and future perspectives, Comput. Struct. Biotechnol. J. 20 (2022) 6578–6585.
[69] P. Barraud, C. Tisne, To be or not to be modified: miscellaneous aspects influencing nucleotide modifications in tRNAs, IUBMB Life 71 (8) (2019) 1126–1140.
[70] S.T. Ahmed, et al., Diagnosis and treatment of mitochondrial myopathies, Neurotherapeutics 15 (4) (2018) 943–953.
[71] A. Nsiah-Sefaa, M. McKenzie, Combined defects in oxidative phosphorylation and fatty acid beta-oxidation in mitochondrial disease, Biosci. Rep. 36 (2) (2016).
[72] B. Jia, et al., The effect of cytoplasmic dynein on the development and functional maintenance of retinal photoreceptor cells, Eur. Rev. Med. Pharmacol. Sci. 25 (21) (2021) 6539–6547.
[73] H.Y. Chen, et al., Primary cilia biogenesis and associated retinal ciliopathies, Semin. Cell Dev. Biol. 110 (2021) 70–88.
[74] T. Ishikawa, Axoneme structure from motile cilia, Cold Spring Harb Perspect Biol 9 (1) (2017).

[75] J. Pasol, Nonorganic visual disorders, Int. Ophthalmol. Clin. 59 (3) (2019) 141–152.
[76] L. Donato, et al., The impact of modifier genes on cone-rod dystrophy heterogeneity: an explorative familial pilot study and a hypothesis on neurotransmission impairment, PLoS One 17 (12) (2022) e0278857.
[77] J.E. Martin-Salazar, D. Valverde, CPLANE complex and ciliopathies, Biomolecules 12 (6) (2022).
[78] L. Laugwitz, et al., Human COQ4 deficiency: delineating the clinical, metabolic and neuroimaging phenotypes, J. Med. Genet. 59 (9) (2022) 878–887.
[79] V.F. Goncalves, Mitochondrial genetics, Adv. Exp. Med. Biol. 1158 (2019) 247–255.
[80] F. Woerz, et al., Interactome analysis reveals a link of the novel ALMS1-CEP70 complex to centrosomal clusters, Mol. Cell. Proteomics 23 (1) (2024) 100701.
[81] D. Gao, et al., Mitochondrial DNA methylation and related disease, Adv. Exp. Med. Biol. 1038 (2017) 117–132.
[82] C. La Morgia, et al., Loss of temporal retinal nerve fibers in Parkinson disease: a mitochondrial pattern? Eur. J. Neurol. 20 (1) (2013) 198–201.
[83] I. Lisovsky, et al., Differential contribution of education through KIR2DL1, KIR2DL3, and KIR3DL1 to antibody-dependent (AD) NK cell activation and ADCC, J. Leukoc. Biol. 105 (3) (2019) 551–563.
[84] R. Kumar, R.A. Wang, Structure, expression and functions of MTA genes, Gene 582 (2) (2016) 112–121.
[85] M. Olahova, et al., POLRMT mutations impair mitochondrial transcription causing neurological disease, Nat. Commun. 12 (1) (2021) 1135.
[86] S. Udhaya Kumar, et al., Comprehensive in silico screening and molecular dynamics studies of missense mutations in Sjogren-Larsson syndrome associated with the ALDH3A2 gene, Adv Protein Chem Struct Biol 120 (2020) 349–377.
[87] Y. Wang, et al., Photoreceptor cell-derived CAPN5 regulates retinal pigment epithelium cell proliferation through direct regulation of SLIT2 cleavage, Invest. Ophthalmol. Vis. Sci. 59 (5) (2018) 1810–1821.
[88] R. Mishal, J.P. Luna-Arias, Role of the TATA-box binding protein (TBP) and associated family members in transcription regulation, Gene 833 (2022) 146581.
[89] J.J. Murray, et al., Leber hereditary optic neuropathy: visual recovery in a patient with the rare m.3890G>A point mutation, J. Neuro Ophthalmol. 37 (2) (2017) 166–171.
[90] J. Chen, et al., mt-Nd2(a) Modifies resistance against autoimmune type 1 diabetes in NOD mice at the level of the pancreatic beta-cell, Diabetes 60 (1) (2011) 355–359.
[91] Q. Xue, et al., Copper metabolism in cell death and autophagy, Autophagy 19 (8) (2023) 2175–2195.
[92] C.G. Tise, et al., MT-ATP6 mitochondrial disease identified by newborn screening reveals a distinct biochemical phenotype, Am. J. Med. Genet. 191 (6) (2023) 1492–1501.